Coupled Wave Theory and Waveguide Applications

By S. E. MILLER

(Manuscript received February 2, 1954)

Some theory describing the behavior of two coupled waves is presented, and it is shown that this theory applies to coupled transmission lines. A loose-coupling theory, applicable when very little power is transferred between the coupled waves, shows how to taper the coupling distribution to minimize the length of the coupling region. A tight-coupling theory, applicable when the coupling is uniform along the direction of wave propagation, shows that a periodic exchange of energy between coupled waves takes place provided that the attenuation and phase constants (α and β respectively) are both equal, or provided that the phase constants are equal and the difference between the attenuation constants ($\alpha_1 - \alpha_2$) is small compared to the coefficient of coupling c. Either ($\alpha_1 - \alpha_2$)/c or ($\beta_1 - \beta_2$)/c being large compared to unity is sufficient to prevent appreciable energy exchange between the coupled waves. Experimental work has confirmed the theory. Applications include highly efficient pure-mode transducers in multi-mode systems, and frequency-selective filters.

INTRODUCTION

This paper describes some theoretical relations in coupled transmission lines, and the use of coupled lines as circuit elements. In order to illustrate the points of interest in the theoretical material, several applications will be stated first. Detailed discussion of experimental models will be given after the theoretical sections.

The theory of coupled transmission lines may be used to determine many properties of a multi-mode transmission system in which there is distributed coupling between modes. In round pipe, for example, the individual modes of propagation can be considered as separate transmission lines which in the perfect waveguide are completely independent. Geometric imperfections in the waveguide, if distributed over many wavelengths, cause a transfer of power between modes which in general

form is predicted by coupled transmission line theory. As a consequence, analysis of the mode-conversion effects associated with circular-electric-wave transmission in commercial round pipe has been aided materially by applying the coupled-transmission-line concept.[1] In another problem, the transmission of the circular-electric waves through bends,[2] the coupled-wave theory of subsequent sections has also provided valuable insight.

Coupled transmission lines can be employed as circuit elements to exchange power between one mode of a multi-mode line and a designated mode of another transmission line. Consider Fig. 1, which shows a rectangular waveguide having entries 1 and 2 coupled through a series of apertures to a parallel round waveguide having entries 3 and 4. The rectangular guide may be made single mode for convenience, and for the configuration shown may be made to couple to any TE mode of the round guide. Input power at entry 1 may be transferred in whole or in part to the selected mode at entry 4, the remaining portion of the power appearing at entry 2. Very little power in any mode will appear at entry 3 for excitation at 1, and very little power in undesired modes will appear at entry 4. Thus the structure has the hybrid property in addition to being mode selective. A matched impedance is presented at all entries to all modes over a very broad frequency band.

Recently, coupled transmission lines have found use as input and output circuits for travelling-wave tubes. In this instance a helical input (or output) line was electromagnetically coupled to the travelling-wave-tube helix, with conditions adjusted for complete energy transfer between the helices. The result is an input-output circuit requiring no metallic connection to the tube helix and requiring no connection through

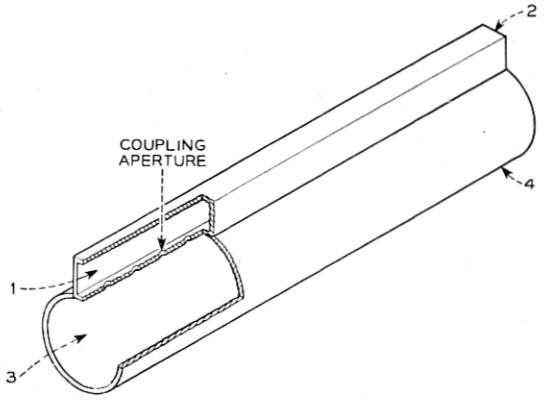

Fig. 1 — Coupled transmission line transducer.

the vacuum seal. R. Kompfner conceived this form of connection to travelling-wave tubes while working with the Admiralty in England, and demonstrated the usefulness of the idea here at the Laboratories. Similar work was done by the group at the Electronics Research Laboratory at Stanford University, and was described by S. T. Kaisel at the August, 1953, West Coast I.R.E. Convention. Both groups requested pre-publication copies of this paper for use in their research.

LOOSE COUPLING THEORY

On the assumption that negligible power is abstracted from the driven line of two coupled transmission lines, the magnitude and mode content of the forward and backward waves in the side line may be written. With reference to Fig. 2, there is assumed coupling between two uniform lines in the interval $-L/2$ to $+L/2$ along the axis of propagation, and no coupling elsewhere. On the basis of loose coupling a normalized voltage wave on line 2 may be written

$$E_2 = 1.0\epsilon^{-i(2\pi/\lambda_2)(x+L/2)}, \tag{1}$$

in which the phase reference is taken as $x = -L/2$. The forward current I_f in the side line at the point $x = L/2$ is

$$I_f = KFM \int_{-\frac{L}{2}}^{\frac{L}{2}} \phi(x)\epsilon^{i2\pi(1/\lambda_1 - 1/\lambda_2)x}\, dx, \tag{2}$$

where

$$F = \frac{\epsilon^{-i\pi L(1/\lambda_1 + 1/\lambda_2)}}{Z_{10}}.$$

$\phi(x)$ = a coupling function. More precisely, $1/\phi(x)$ is the ratio of the voltage on line 2, $E_2(x)$, to the equivalent voltage generator in series with line 1 at x.

K = fraction of the transferred current which travels in the forward direction.

M = the transfer constant for the various modes which can propagate, relative to the mode for which $\phi(x)$ is defined. The backward current I_b at the point $x = -L/2$ is

$$I_b = (1 - K)FM \int_{-\frac{L}{2}}^{\frac{L}{2}} \phi(x)\epsilon^{-i2\pi(1/\lambda_1 + 1/\lambda_2)x}\, dx. \tag{3}$$

If the coupling mechanism is non-directive (sending equal waves forward and backward) and has the same value for all modes, then $K = \frac{1}{2}$ and $M = 1.0$. For simplicity these values are assumed in writing the remainder of the expressions. However, the theory is applicable if the coupling mechanism is mode selective and/or directive provided that these properties do not change over the length of the coupling interval.

The mode discriminating property of the coupled lines is the ratio of the forward current for $\lambda_1 = \lambda_2$ to the forward current for $\lambda_1 \neq \lambda_2$. This ratio is

$$\text{Discrimination} = \left| \frac{I_f\ (\lambda_1 = \lambda_2)}{I_f\ (\lambda_1 \neq \lambda_2)} \right| = \frac{\int_{-\frac{L}{2}}^{\frac{L}{2}} \phi(x)\, dx}{\int_{-\frac{L}{2}}^{\frac{L}{2}} \phi(x) \epsilon^{i\frac{2\theta}{L}x}\, dx}, \tag{4}$$

where $\theta = \pi L(1/\lambda_1 - 1/\lambda_2) = L(\beta_1 - \beta_2)/2$ and the β's are the phase constants of the two transmission lines.

The directivity of the coupling arrangement is defined as the ratio of the forward current for $\lambda_1 = \lambda_2$ to the backward current; this ratio is also given by equation (4) provided

$$\theta = -\pi L \left(\frac{1}{\lambda_1} + \frac{1}{\lambda_2} \right) = -\frac{L}{2} (\beta_1 + \beta_2).$$

Thus, in the loose coupling case, the critical performance characteristics are given by the discrimination function, equation (4), for appropriate values of the parameter θ.

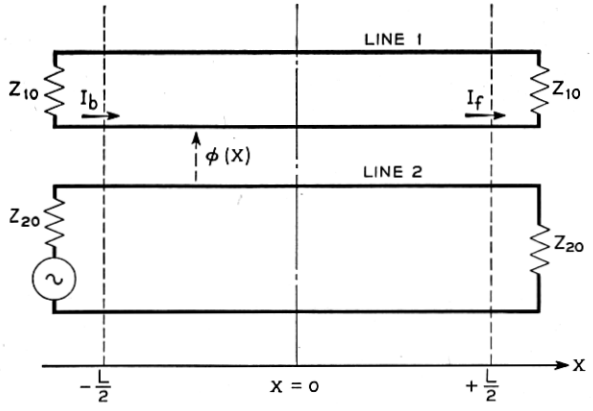

Fig. 2 — Schematic of coupled transmission lines.

A simplified example will illustrate the application of these relations. Suppose the coupling function $\phi(x)$ is constant in the interval $-L/2$ to $L/2$ and zero for other values of x. Then the discrimination function is, from (4)

$$\text{Uniform Coupling Discrimination} = \frac{\theta}{\sin \theta}. \tag{5}$$

Let us further assume, in the hypothetical example, that line 2 (Fig. 2) is a single-mode line having a guide wavelength λ_2 equal to $1.2\lambda_0$, and that line 1 is the three-mode line having guide wavelengths λ_1, λ_2, and λ_3 equal to $1.1\lambda_0$, $1.2\lambda_0$, and $1.3\lambda_0$ respectively. Assume the coupling length L equals $20\lambda_0$. For equal coupling to all modes in a differential unit of length, the relative current waves travelling in the forward direction in the three modes of line 1 are obtained from (4). For the ratio of the λ_2 forward current to the λ_1 forward current,

$$\theta = \pi 20\lambda_0 \left(\frac{1}{1.1\lambda_0} - \frac{1}{1.2\lambda_0} \right) = 1.52\pi$$

for which (5) gives a discrimination of about 13.5 db. For the ratio of the λ_2 forward current to the λ_3 forward current

$$\theta = \pi 20\lambda_0 \left(\frac{1}{1.2\lambda_0} - \frac{1}{1.3\lambda_0} \right) = 1.28\pi,$$

corresponding to a discrimination of about 14 db. For the ratio of the λ_2 forward current to the λ_2 backward current,

$$\theta = \pi 20\lambda_0 \left(\frac{1}{1.2\lambda_0} + \frac{1}{1.2\lambda_0} \right) = 33.3\pi,$$

corresponding to a discrimination of about 43 db. The backward currents in modes λ_1 and λ_3 can similarly be verified to be very small compared to the forward-travelling λ_2 current.

Thus, directivity and mode purity in a simplified case have been shown to be of the desired form.

It may be noted that the denominator of (4) is the Fourier transform of the coupling function $\phi(x)$. Since the numerator of (4) is independent of θ, the discrimination is maximized by minimizing the denominator. An analogous problem exists in the time versus frequency domain relations, and experience with the latter can be used to predict the discriminations to be expected using various coupling distributions.

In the simple example cited above, a length of coupling interval of $20\lambda_0$ yielded a discrimination between the desired versus undesired for-

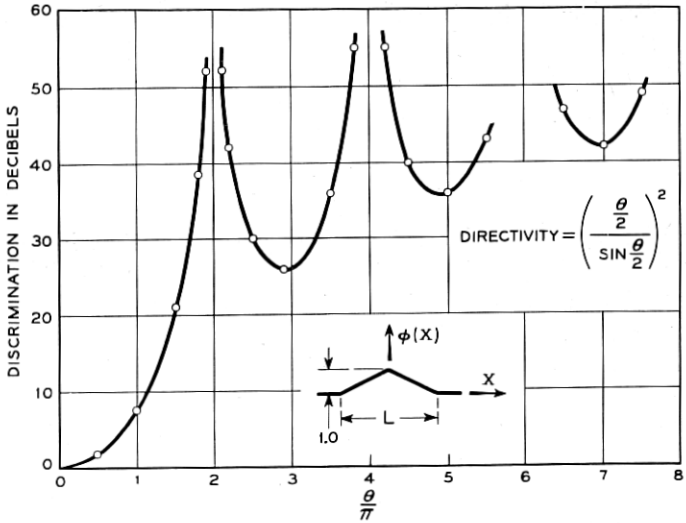

Fig. 3 — Discrimination versus θ/π for linear taper coupling.

ward wave components of about 13 db. How can this discrimination be improved? If the difference between the wavelengths of the desired and undesired wave types is increased, the value of θ is increased and greater discrimination results. In practical cases, however, there frequently is very little that can be done about the wavelength difference because it is inherent in a structure which is fixed by other considerations. By increasing the length of the coupling interval L the value of θ is also increased; in the case of uniform coupling, (5) shows that a value of θ/π equal to about 8 is required to get 30 db discrimination. In the above example this corresponds to L approximately equal to $125\lambda_0$. The latter coupling length is probably impractical, and is certainly inconvenient. The final alternative is to alter the distribution of coupling between the lines, and considerable can be done in this manner.

Suppose a linear taper of the strength of coupling is used, as sketched in Fig. 3. Then the discrimination becomes

$$\text{Linear Taper Discrimination} = \left(\frac{\theta/2}{\sin \theta/2}\right)^2. \tag{6}$$

which is plotted in Fig. 3. The first peak in discrimination occurs at θ/π equals two, compared to a value of θ/π equals one for the first peak using uniform coupling; however, for all values of θ/π greater than about 3, the linear taper provides superior discrimination. This illustrates a general trend; tapering the coupling distribution improves the discrimina-

tion for large θ/π values at the expense of an increased θ/π value for the first discrimination peak.

The first two lines of Fig. 4 give the discrimination functions for two forms of cosine taper; Fig. 5 shows a plot of the first function and Fig. 6 shows a plot of the second function for a particular case. These figures illustrate the importance of the slope at the ends of the coupling distribution. Comparing Fig. 5 with Fig. 3, Fig. 5 has a larger end-slope, shows a lower value of θ/π for the first peak in discrimination, but provides

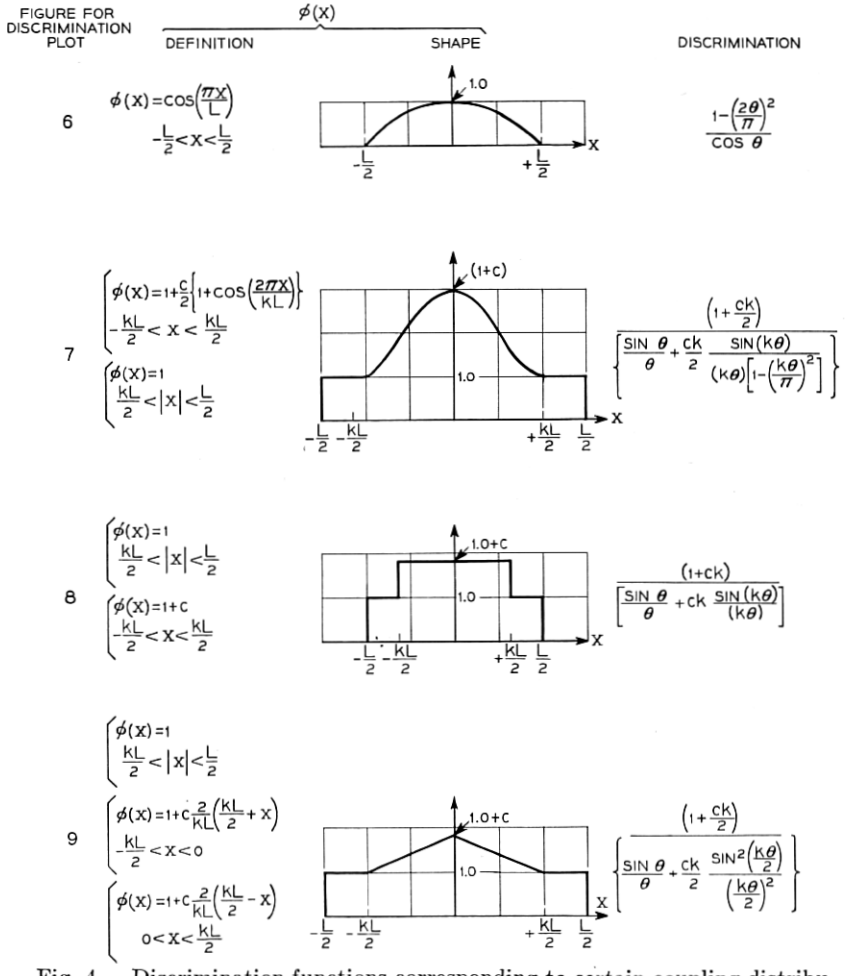

Fig. 4 — Discrimination functions corresponding to certain coupling distributions.

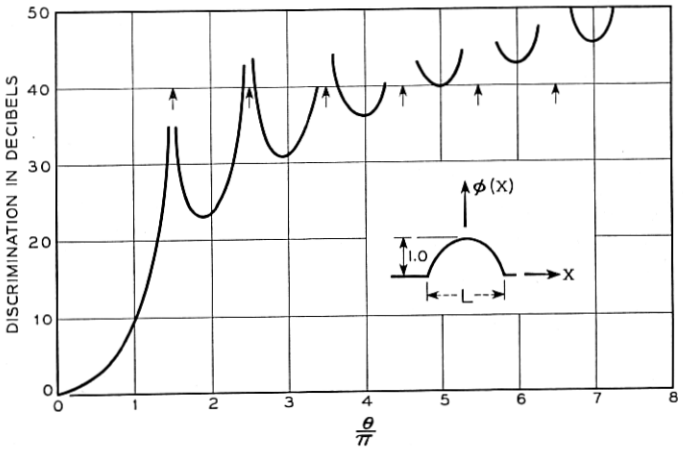

Fig. 5 — Discrimination versus θ/π for the cosine coupling disbribution.

poorer discrimination at values of θ/π slightly above the first peak. In a similar way Fig. 6 shows better discrimination than Fig. 5.

Linear superposition of forward or backward currents may be employed to advantage when designing a coupling distribution. The second line of Fig. 4 gives the discrimination for a coupling function composed of a raised cosine plus uniform coupling. For a value of $c = 22.4$ and $k = 1$,

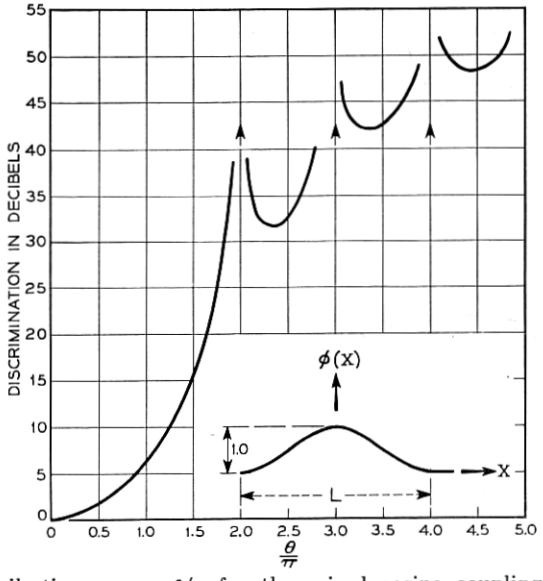

Fig. 6 — Distribution versus θ/π for the raised cosine coupling distribution.

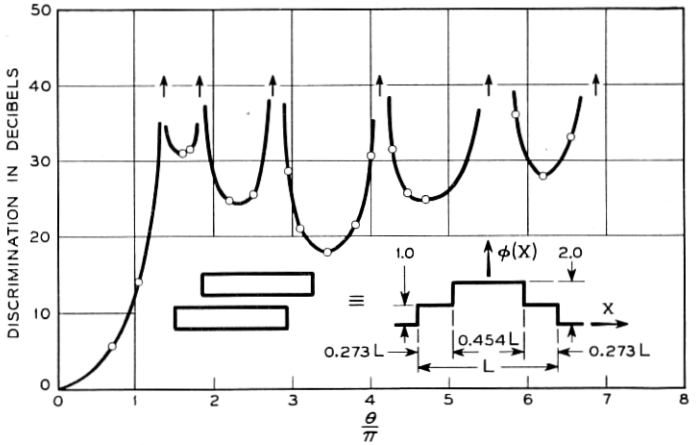

Fig. 7 — Discrimination versus θ/π for two uniform couplings superposed.

the discrimination is greater than 38 db for θ/π between 1.95 and 3.0, and is greater than 50 db for θ/π larger than 3. Below $\theta/\pi = 1.95$ the discrimination is similar to that shown in Fig. 6.

Linear superposition of two uniform coupling distributions yields a structure which is easy to fabricate and, in cases where the requirements are not too complex, may provide satisfactory discrimination. The third line of Fig. 4 gives the general relation, and Fig. 7 shows the discrimination plot for a case of interest. Discriminations on the order of 30 db are available in a broad region between θ/π equal to 1.3 to 2, an attractive abscissa value compared to the $\theta/\pi = 8$ required for simple uniform coupling.

Linear superposition of a linear taper and uniform coupling also yields a structure which is easy to fabricate, and the theoretical discrimination plot for an interesting set of conditions is shown in Fig. 8. High discriminations are provided over greater ranges of θ than for the case of two uniform coupling functions superposed.

The general relations involved in the superposition of coupling functions may be summarized as follows: Let $\phi_1(x), \phi_2(x) \cdots \phi_n(x)$ be known coupling functions and let

$$\phi_T = \phi_1 + \phi_2 + \cdots \phi_n . \tag{7}$$

Let the maximum length of the coupling interval be L. Then, designating the transforms of $\phi_1, \phi_2 \cdots \phi_n$ by F_1 and $F_2 \cdots F_n$ respectively, where

$$F_n = \int_{-L/2}^{L/2} \phi_n(x) \epsilon^{i(2\theta/L)x} \, dx, \tag{8}$$

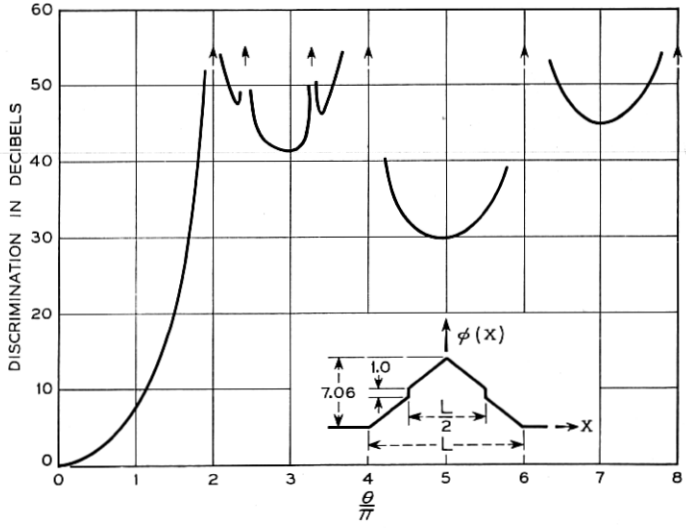

Fig. 8 — Discrimination versus θ/π for a linear taper and uniform coupling superposed.

and letting

$$F_T = F_1 + F_2 + \cdots F_n , \tag{9}$$

the discrimination function for the composite coupling distribution $\phi_T(x)$ is given by

$$\text{Discrimination} = \frac{F_T(\theta = 0)}{F_T} . \tag{10}$$

Another useful theoretical approach to the employment of multiple distributed coupling functions is illustrated in Fig. 9. The top sketch represents any coupling function $\phi_1(x)$. The lower sketch shows a new coupling function $\phi_2(x)$ formed by locating a $\phi_1(x)$ at $\pm d/2$ on the "x" axis. Using F_1 to denote the transform for $\phi_1(x)$, and F_2 to denote the transform corresponding to $\phi_2(x)$,

$$F_2 = 2F_1 \cos \theta' , \tag{11}$$

wherein

$$\theta' = d\left(\frac{1}{\lambda_1} - \frac{1}{\lambda_2}\right)$$

for the forward wave discrimination and

$$\theta' = d\left(\frac{1}{\lambda_1} + \frac{1}{\lambda_2}\right)$$

for the directivity as defined earlier in connection with (4).

The discrimination function for the composite coupling function $\phi_2(x)$ is

$$\text{Discrimination} = \frac{F_2(\theta = 0, \theta' = 0)}{F_2} = \frac{F_1(\theta = 0)}{F_2}\frac{1}{\cos\theta'}. \quad (12)$$

The factor $1/\cos\theta'$ is the discrimination function associated with two point couplings, and the overall discrimination is the *product* of that discrimination and the discrimination associated with a single distributed coupling function $\phi_1(x)$. This line of thought may be extended to show that use of the same *distributed* coupling function in place of each point coupling in the multi-element distributions described in the following section results in multiplying the discrimination of the multi-element coupling function by the discrimination associated with the distributed coupling function.

In many cases of interest it is either inconvenient or impossible to use absolutely continuous coupling between transmission lines. In the waveguide case illustrated in Fig. 1, for example, a continuous slot cut in the common wall would not provide coupling of the distributed form due to a wave which would oscillate back and forth in the slot itself. We know, however, that the effects of the continuous coupling distribution can be

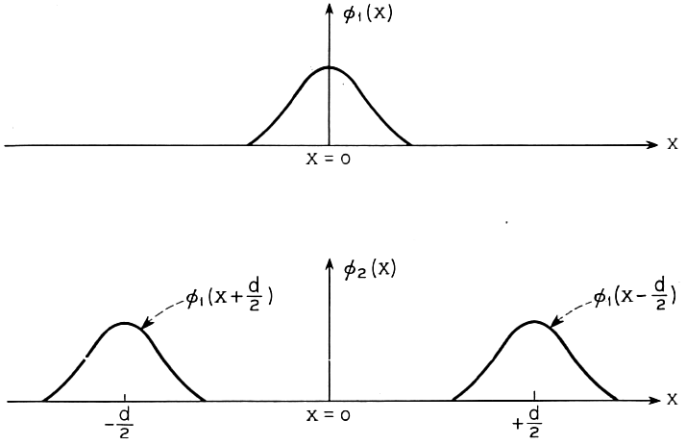

Fig. 9 — Schematic of multiple distributed coupling functions.

simulated closely by using closely spaced point couplings. In order to do this intelligently we need a theory for multi-element point couplings.

The most general symmetrical point coupling distribution for parallel coupled lines is illustrated in Fig. 10. The letters a_0, a_1, $a_2 \cdots a_n$ designate the strength of the couplings, and d_1, d_2, $\cdots L$ represents the spacings between them. The transform for the total coupling distribution is

$$F_T = \int_{-L/2}^{L/2} \phi_T \epsilon^{i(2\theta x/L)}\, dx. \tag{13}$$

$F_T = a_0 + 2a_1 \cos \gamma_1 + 2a_2 \cos \gamma_2 + 2a_3 \cos \gamma_3 + \cdots 2a_n \cos \theta$ in which

$$\gamma_k = \pi d_k \left(\frac{1}{\lambda_1} - \frac{1}{\lambda_2}\right) \text{ or } \pi d_k \left(\frac{1}{\lambda_1} + \frac{1}{\lambda_2}\right),$$

and

$$\theta = \pi L \left(\frac{1}{\lambda_1} - \frac{1}{\lambda_2}\right) \text{ or } \pi L \left(\frac{1}{\lambda_1} + \frac{1}{\lambda_2}\right),$$

depending on whether forward wave discrimination or directivity is required. The discrimination function is then

$$\text{Discrimination} = \frac{F_T(\gamma_k = 0, \theta = 0)}{F_T}. \tag{14}$$

Let us take as an example the familiar 1–3–3–1 binomial distribution of amplitudes for equally spaced couplings. In the terminology of equation (13), $a_0 = 0$, $a_1 = 3$, $a_2 = 1$, $a_k = 0$ for $k > 2$, $d_1 = L/3$, and $d_2 = L$. Then (14) yields

$$\text{Discrimination} = \frac{8}{6 \cos \theta/3 + 2 \cos \theta} = \frac{1}{\cos^3 \theta/3}. \tag{15}$$

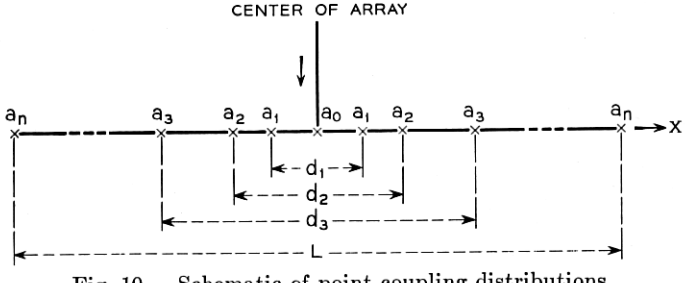

Fig. 10 — Schematic of point coupling distributions.

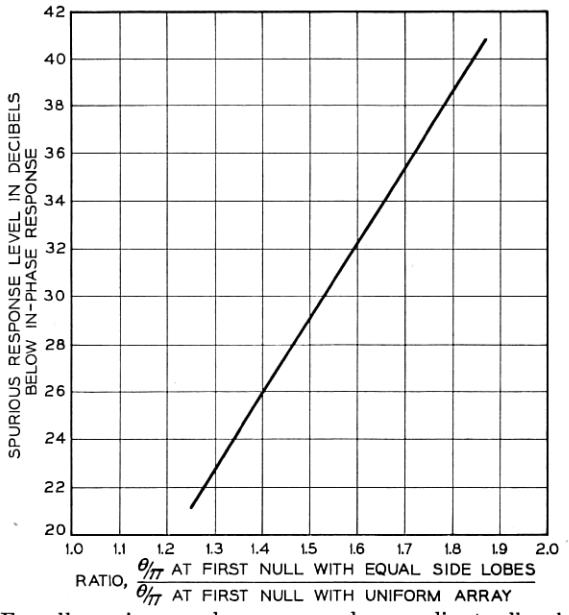

Fig. 11 — For all spurious mode responses down ordinate db, abscissa is the ratio of the required coupling length to the length required for constant amplitude coupling to produce a first null at the same value of $(1/\lambda_1 - 1/\lambda_2)$. (After C. L. Dolph, Reference 4).

which is the relation given by Mumford.[3] The approach is perfectly general, and henceforth the coupling distribution only will be given with the understanding that the corresponding discrimination function can be obtained from (13) and (14).

For the case of tapered amplitudes and an even number of equally spaced couplings, (13) can be simplified to

$$F_T = 2a_1 \cos\left(\frac{\theta}{2n-1}\right) + 2a_2 \cos\left(\frac{3\theta}{2n-1}\right) + \cdots 2a_n \cos 6. \quad (16)$$

This case is of interest because a solution has been worked out for the analogous antenna problem to bring the spurious responses (the peaks of the side lobes in the antenna case, or the peaks of the undesired mode responses in the wave selector case) to the same level relative to the desired response. *This makes the total length of the coupling array a minimum for a given required degree of discrimination.* The solution[4] includes specification of the Tchebysheff distribution of coupling strengths a_1, a_2, $a_3 \cdots a_n$ that are required to achieve various levels of spurious response, and the resulting increase in total array length required to place the first null

in undesired mode response at the same value of

$$\left(\frac{1}{\lambda_1} - \frac{1}{\lambda_2}\right) \text{ or } \left(\frac{1}{\lambda_1} + \frac{1}{\lambda_2}\right)$$

as for uniform strength couplings equally spaced. Fig. 11 shows the latter relation, a very useful yardstick with which to evaluate the extra coupling length required by less ideal but more easily constructed coupling distributions.

An important practical question is "What is the smallest number of point couplings which will satisfy requirements in a given stiuation?", for it is time-consuming and expensive to fabricate the coupling holes or probes in some circumstances. The large range of possible mode conditions and discrimination requirements makes it difficult to give an answer in closed form, but the general restrictions involved may be stated. In the case of n equally spaced couplings (of any amplitude taper) the discrimination vanishes at $\theta/\pi = (n - 1)$. This is illustrated by the discrimination plot of Fig. 12.

Moreover, it is found that equally spaced couplings produce discriminations which are periodic in θ/π on the interval $(n - 1)$, and which are symmetrical about $\theta/\pi = (n - 1)/2$.

The implication of the discrimination zero at $\theta/\pi = (n - 1)$ is that a large number of point couplings are required to get good directivity and good forward wave discrimination. In the simple case cited above in which $L = 20\lambda_0$, the θ/π value for directivity was shown to be 33.3.

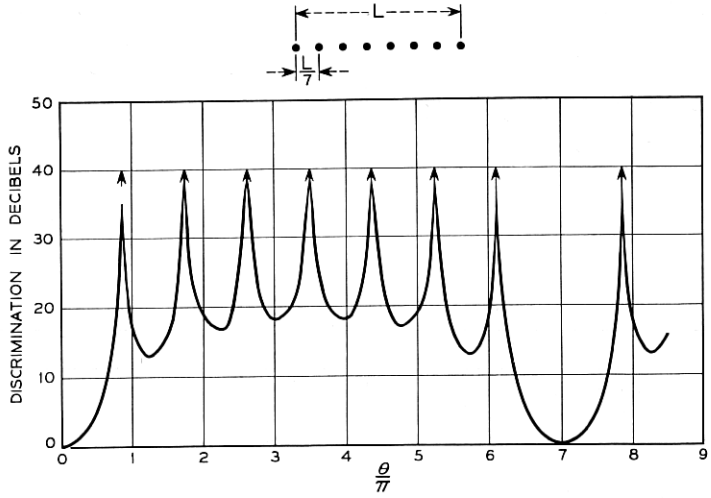

Fig. 12 — Discrimination for 8 equal-strength point couplings equally spaced.

Thus, something on the order of 50 or 60 equally spaced couplings might be needed.

Simulation of continuous coupling functions with equal strength couplings may be carried out as follows: the coupling amplitude versus distance plot may be divided along the distance axis into a number of intervals of equal area, and a point coupling placed at the center of each interval. The more efficient continuous coupling functions require more point couplings to get a good simulation in this manner. For example, the function of line 2, Fig. 4, with $c = 22.4$ and $k = 1$ has been simulated with 12 and 40 equal strength couplings (as described above) and the exact discrimination plotted using (13) and (14). The results are given in Figs. 13 and 14. The original continuous coupling function yields discriminations greater than 38 db for all values of θ/π greater than 2; the 40-point simulation approximates this well in the region of $\theta/\pi = 1.7$ to 4.5, but thereafter begins to fail. The 12-point simulation (Fig. 13) never matches the original but does best in the region of small θ/π.

It is more efficient to seek high discriminations by tapering the strength of equally spaced couplings than by tapering the spacing between equal strength couplings. However, when low discriminations are acceptable, the relative efficiency of tapering the spacing between con-

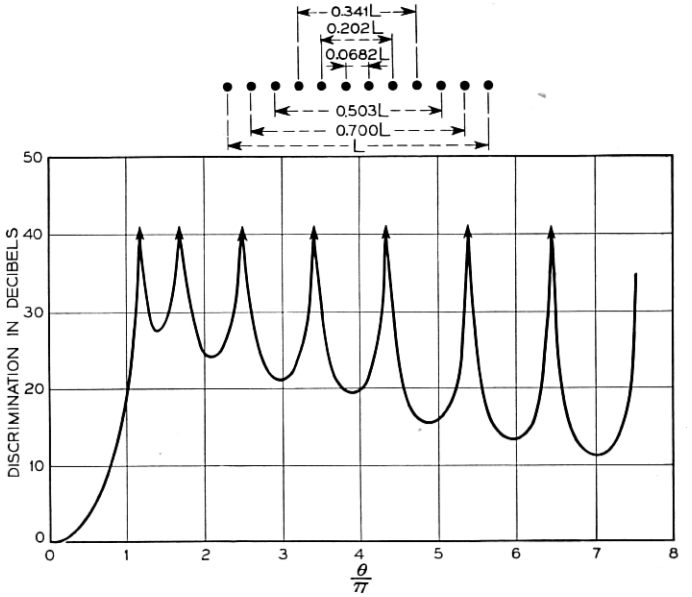

Fig. 13 — Discrimination for 12 equal-strength point couplings arranged to simulate the continuous distribution of Fig. 4, line 2.

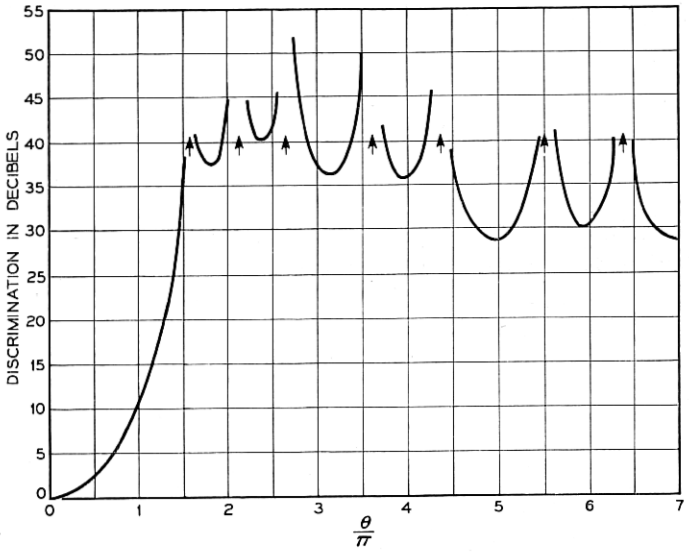

Fig. 14 — Discrimination for 40 equal-strength point couplings arranged to simulate the continuous distribution of Fig. 4, line 2.

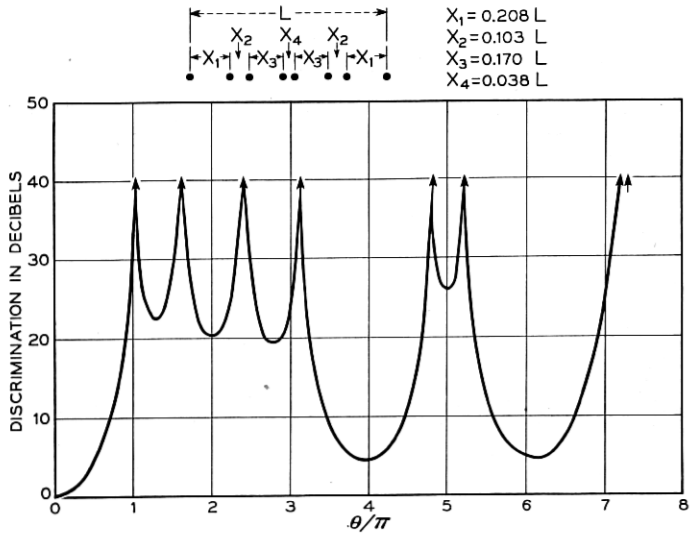

Fig. 15 — Discrimination function for 8 equal strength couplings arranged to maximize the bandwidth (θ/π range) for moderate discrimination.

stant strength couplings is much greater than when high discriminations are required. Fig. 15 shows a distribution which produces about 20 db discrimination from $\theta/\pi = 1$ to 3.25. Eight couplings arranged with the Tchebysheff amplitude taper for 20 db discrimiuation would produce that discrimination from $\theta/\pi = 1.05$ to 5.95.

It is possible to obtain directivity or mode discrimination at smaller θ/π values than made available with uniform coupling. This situation is analogous to the superdirectivity problem in antenna design, with similar results — the lobes of spurious response are increased. In particular, if the coupling near the ends of the third array of Fig. 4 is made larger than the coupling in the center region, making "c" a negative quantity, the first peak in discrimination occurs at θ/π less than one, and the first minimum in discrimination becomes less than 13 db.

By implication, emphasis has been placed on obtaining both mode discrimination and directivity simultaneously. However, by employing a relatively short coupling length it is apparent that the discrimination associated with

$$\theta = \pi L \left(\frac{1}{\lambda_1} - \frac{1}{\lambda_2} \right)$$

may be kept small when the directivity associated with

$$\theta = \pi L \left(\frac{1}{\lambda_1} + \frac{1}{\lambda_2} \right)$$

is in suitable range for good discrimination. Consequently, one can design a directional coupler with little mode discrimination. Conversely, when using a relatively small number of point couplings, the mode discrimination in the forward wave may be good when the directivity is poor.

TIGHT COUPLING THEORY*

We now consider the case in which a significant amount of power is taken from the driven transmission line by the line coupled to it. To simplify the problem the coupling is assumed uniform along the length

* An analysis of coupled transmission lines was given by W. J. Albersheim,[11] and the effects of coupling between waves on certain particular forms of transmission media were analyzed by Meyerhoff[9] and Krasnushkin and Khokhlov.[10] The treatment given here is intended to be more general and is believed to describe the effects of wave coupling under a greater variety of conditions.

axis. The space variation of the wave amplitude may be written

$$\frac{dE_1}{dx} = -(\Gamma_1 + k_{11})E_1 + k_{21}E_2 , \tag{17}$$

and

$$\frac{dE_2}{dx} = k_{12}E_1 - (\Gamma_2 + k_{22})E_2 , \tag{18}$$

in which k_{11} , k_{22} represent the reaction of the coupling mechanism on lines 1 and 2 respectively

k_{21} , k_{12} represent the transfer effects of the coupling mechanism

$\Gamma_{1,2}$ are the uncoupled propagation constants of line 1 and 2 respectively;

$E_{1,2}$ are the complex wave amplitudes on lines 1 and 2,

and are so chosen that $| E_1 |^2$ and $| E_2 |^2$ represent the power carried by lines 1 and 2 respectively at the input or output of the coupling region. The usual transmission-line equations are of this general form, except for second derivatives in place of the first. The first derivatives appear here because we deal only with the forward travelling waves, which the preceding section has shown are the only significant waves when small coupling per wave length is employed. Limiting our interest to the cases for which reciprocity holds and noting that there is always a transverse plane of symmetry midway between the ends of any pair of uniformly coupled lines, we may transform the wave amplitudes to make $k_{12} = k_{21} = k$. We may further simplify the equations without loss of essential generality by submerging the differences $(k_{11} - k)$ and $(k_{22} - k)$ into a modified propagation constant for lines 1 and 2 respectively, yielding

$$\frac{dE_1}{dx} = -(\gamma_1 + k)E_1 + kE_2 , \tag{19}$$

and

$$\frac{dE_2}{dx} = kE_1 - (\gamma_2 + k)E_2 , \tag{20}$$

in which

$$\begin{aligned} \gamma_1 &= \Gamma_1 + k_{11} - k, \qquad \text{and} \\ \gamma_2 &= \Gamma_2 + k_{22} - k. \end{aligned} \tag{20'}$$

For some cases $k_{11} = k_{22} = k$ and for all cases of interest here γ_n differs very little from Γ_n since we are concerned only with loose coupling per wavelength.

The solution, for $E_1 = 1.0$ and $E_2 = 0$ at $x = 0$, is

$$E_1 = \left[\frac{1}{2} - \frac{(\gamma_1 - \gamma_2)}{2\sqrt{(\gamma_1 - \gamma_2)^2 + 4k^2}}\right] \epsilon^{r_1 x} + \left[\frac{1}{2} + \frac{(\gamma_1 - \gamma_2)}{2\sqrt{(\gamma_1 - \gamma_2)^2 + 4k^2}}\right] \epsilon^{r_2 x}, \tag{21}$$

and

$$E_2 = \frac{k}{\sqrt{(\gamma_1 - \gamma_2)^2 + 4k^2}} \epsilon^{r_1 x} - \frac{k}{\sqrt{(\gamma_1 - \gamma_2)^2 + 4k^2}} \epsilon^{r_2 x}, \tag{22}$$

where

$$r_1 = -\tfrac{1}{2}(2k + \gamma_1 + \gamma_2) + \tfrac{1}{2}\sqrt{(\gamma_1 - \gamma_2)^2 + 4k^2}, \tag{23}$$

$$r_2 = -\tfrac{1}{2}(2k + \gamma_1 + \gamma_2) - \tfrac{1}{2}\sqrt{(\gamma_1 - \gamma_2)^2 + 4k^2}. \tag{24}$$

The nature of the coupling coefficient k is the first thing to investigate. Assume no dissipation in either the transmission line or in the coupling mechanism. Then it follows that for any value of x,

$$|E_1|^2 + |E_2|^2 = \text{constant} \tag{25}$$

on the basis of energy conservation. It may be determined that (25) leads to the requirement that the coupling constant k be purely imaginary. This is a very important result. In all of the following discussion k is taken to be purely imaginary. Even where dissipation in the transmission lines themselves is important, it is still assumed that the coupling mechanism is non-dissipative.

The simplest case is $\gamma_1 = \gamma_2 = \gamma$, coupling between identical transmission lines. Then (21) and (22) reduce to

$$E_1 = \cos cx \; \epsilon^{-(ic+\gamma)x}, \tag{26}$$

and

$$E_2 = i \sin cx \; \epsilon^{-(ic+\gamma)x}, \tag{27}$$

where $k = ic$. The exponential of (26) and (27) shows that the coupling modifies the average phase constant, and that the attenuation in the driven line (E_1) is the same as in the uncoupled case for cx (coupling length times coupling strength) equal to $n\pi$ radians. The amplitude and phase variations due to the coupling are plotted in Fig. 16. Complete power transfer between lines takes place cyclically, with a period of $cx = \pi$, and with suitable choice of the product cx, an arbitrary division of power between the lines may be selected.

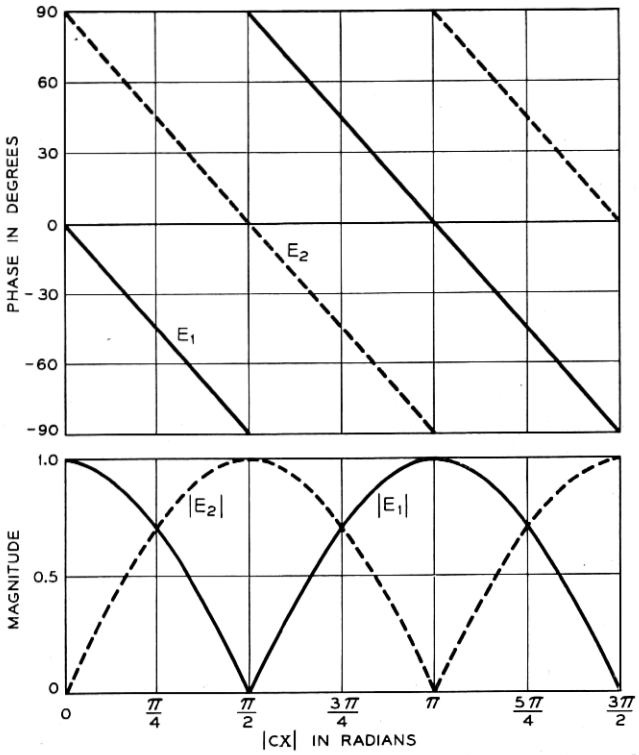

Fig. 16 — Wave amplitude and phase factors versus the integrated coupling strength cx for tightly coupled transmission lines having identical propagation constants.

Let us now assume that the phase constants of the two lines are unequal, but the attenuation constants are the same. Then

$$\alpha_1 = \alpha_2 = \alpha, \qquad \text{and}$$
$$(\gamma_1 - \gamma_2) = i(\beta_1 - \beta_2), \tag{28}$$

and equations (21) and (22) reduce to

$$E_1 = \epsilon^{-[\alpha + i(c + (\beta_1 + \beta_2)/2)]x} E_1^*, \tag{29}$$

where

$$E_1^* = \cos\left[\sqrt{\frac{(\beta_1 - \beta_2)^2}{4c^2} + 1}\, cx\right] - \frac{i(\beta_1 - \beta_2)}{2c} \frac{1}{\sqrt{\frac{(\beta_1 - \beta_2)^2}{4c^2} + 1}} \sin\left[\sqrt{\frac{(\beta_1 - \beta_2)^2}{4c^2} + 1}\, cx\right] \tag{30}$$

$$E_2 = \epsilon^{-[\alpha + i(c + (\beta_1 + \beta_2)/2)]x} E_2^* \tag{31}$$

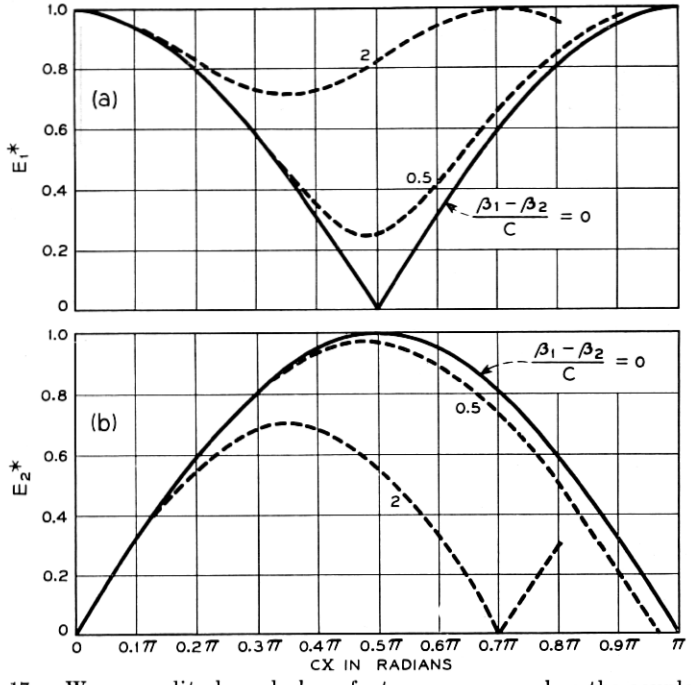

Fig. 17 — Wave amplitude and phase factors versus cx when the coupled lines have equal attenuation constants but unequal phase constants.

where

$$E_2^* = \frac{1 \quad i}{\sqrt{\frac{(\beta_1 - \beta_2)^2}{4c^2} + 1}} \sin\left[\sqrt{\frac{(\beta_1 + \beta_2)^2}{4c^2} + 1}\, cx\right] \tag{32}$$

The major effects of coupling in this case are represented by E_1^* and E_2^*, which are plotted in Fig. 17 for several values of $(\beta_1 - \beta_2)$. As $(\beta_1 - \beta_2)$ becomes different from zero, the maximum power transferred from the driven line to the undriven line decreases, and the period of the cyclical variation in amplitude is reduced. The latter period is the value of cx given by

$$\sqrt{\frac{(\beta_1 - \beta_2)^2}{4c^2} + 1}\, cx = \pi \tag{33}$$

The driven and undriven-line wave amplitudes E_1^* and E_2^* at the maximum power transfer point, namely, at

$$\sqrt{\frac{(\beta_1 - \beta_2)^2}{4c^2} + 1}\, cx = \frac{\pi}{2} \tag{34}$$

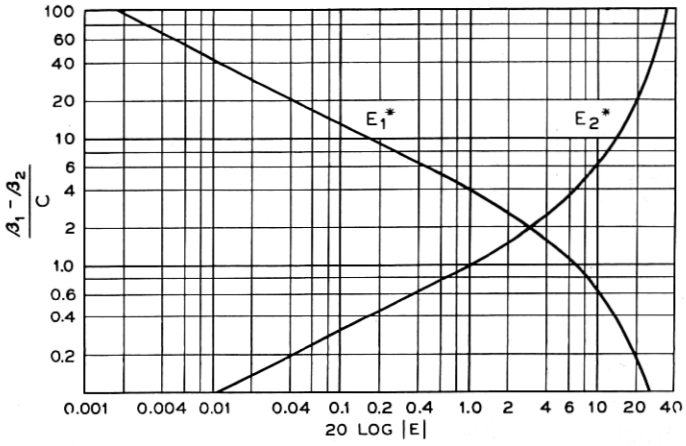

Fig. 18 — Wave amplitude factors at the maximum power transfer value of cx versus $(\beta_1 - \beta_2)/c$ when the coupled lines have equal attenuation constants.

are plotted in Fig. 18 as a function of the ratio $(\beta_1 - \beta_2)/c$. It is evident that this maximum energy transfer may be made very small for suitably large values of $(\beta_1 - \beta_2)/c$. The behavior of E_1^* and E_2^* as a function of coupling length x is shown with greater accuracy in the wide amplitude range of interest in Figures 19 and 20 respectively.

Consider now the case in which the coupled lines have identical phase constants, $\beta_1 = \beta_2 = \beta$, and unequal attenuation constants so that $(\gamma_1 - \gamma_2) = (\alpha_1 - \alpha_2)$. Then (21) and (22) reduce to

$$E_1 = \epsilon^{-[\alpha_1 + i(c+\beta)]x} \left\{ \left[\frac{1}{2} - \frac{(\alpha_1 - \alpha_2)}{2\sqrt{(\alpha_1 - \alpha_2)^2 - 4c^2}} \right] \epsilon^{\left[(\alpha_1 - \alpha_2)/2 + \frac{1}{2}\sqrt{(\alpha_1 - \alpha_2)^2 - 4c^2}\right]x} + \left[\frac{1}{2} + \frac{(\alpha_1 - \alpha_2)}{2\sqrt{(\alpha_1 - \alpha_2)^2 - 4c^2}} \right] \epsilon^{\left[(\alpha_1 - \alpha_2)/2 - \frac{1}{2}\sqrt{(\alpha_1 - \alpha_2)^2 - 4c^2}\right]x} \right\}, \tag{35}$$

$$E_1 = \epsilon^{-[\alpha_1 + i(c+\beta)]x} E_1^{**}, \tag{35'}$$

and

$$E_2 = \epsilon^{-[\alpha_1 + i(c+\beta)]x} \frac{ic}{\sqrt{(\alpha_1 - \alpha_2)^2 - 4c^2}} \left\{ \epsilon^{\left[(\alpha_1 - \alpha_2)/2 + \frac{1}{2}\sqrt{(\alpha_1 - \alpha_2)^2 - 4c^2}\right]x} - \epsilon^{\left[(\alpha_1 - \alpha_2)/2 - \frac{1}{2}\sqrt{(\alpha_1 - \alpha_2)^2 - 4c^2}\right]x} \right\}, \tag{36}$$

or

$$E_2 = \epsilon^{-[\alpha_1 + i(c+\beta)]x} E_2^{**}. \tag{36'}$$

The amplitude factors E_1^{**} and E_2^{**} have been defined in such a way as to reflect the principal effects of *attenuation difference* in the two lines; for the case in which the driven line attenuation constant α_1 is negligible, note that E_1^{**} and E_2^{**} contain all the amplitude variations of E_1 and E_2 respectively. In general, E_1^{**} and E_2^{**} are the ratios of the wave amplitudes actually present in lines 1 and 2 respectively to the wave amplitude which would exist in line 1 at the same value of x in the absence of coupling.

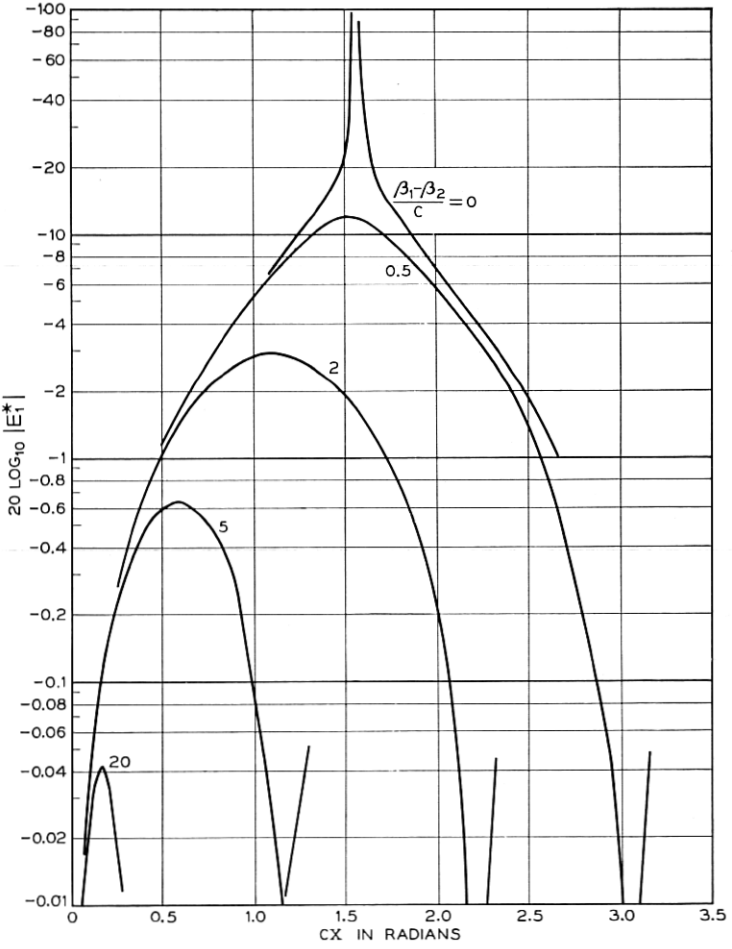

Fig. 19 — Driven line wave amplitude versus cx with unequal phase constants and equal attenuation constants. The curves are periodic for larger values of cx.

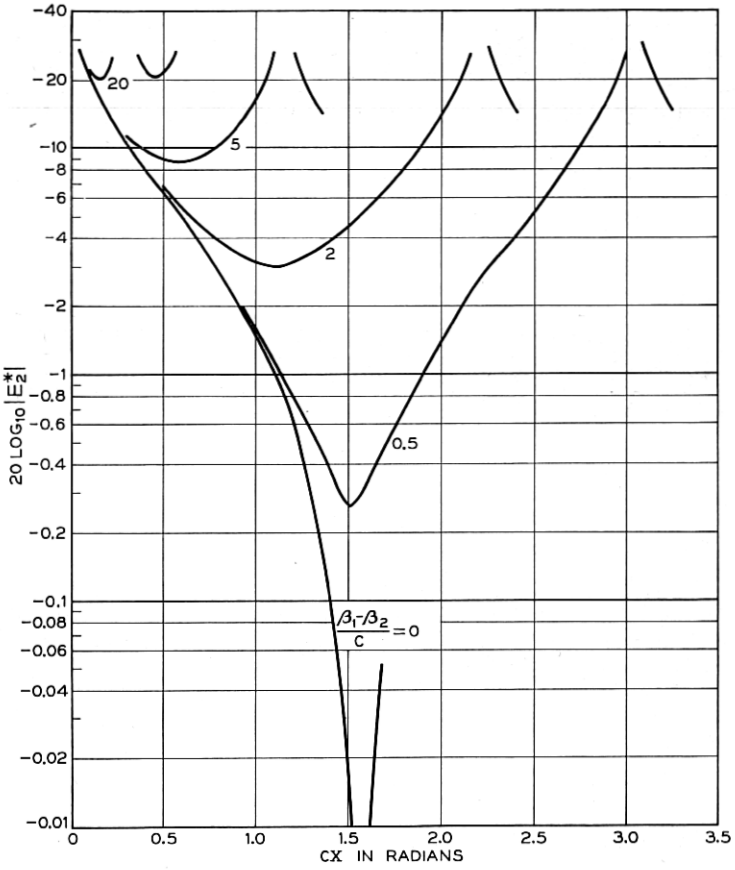

Fig. 20 — Undriven line wave amplitude versus cx with unequal phase constants and equal attenuation constants. The curves are periodic for larger values of cx.

We consider first the case of $(\alpha_1 - \alpha_2)$ negative, i.e., a lower attenuation constant inthe driven line than in the undriven line. The effects of unequal attenuation constants may be illustrated at the integrated coupling strength $cx = \pi/2$ which, as Fig. 16 shows, results in complete transfer of power to the undriven line when $\alpha_1 = \alpha_2$ and $\beta_1 = \beta_2$. Fig. 21 shows that the driven line wave amplitude E_1^{**} is very small when $(\alpha_1 - \alpha_2)/c$ is small, but is only ¼ db below unity when $(\alpha_1 - \alpha_2)/c$ is about 55. Fig. 22 illustrates the way the undriven line wave amplitude E_2^{**} decreases as $(\alpha_1 - \alpha_2)/c$ increases.

For integrated coupling strengths less than $\pi/2$, the effects of unequal attenuation constants are not pronounced at small $(\alpha_1 - \alpha_2)/c$, but again for large $(\alpha_1 - \alpha_2)/c$, E_1^{**} approaches unity and E_2^{**} becomes small.

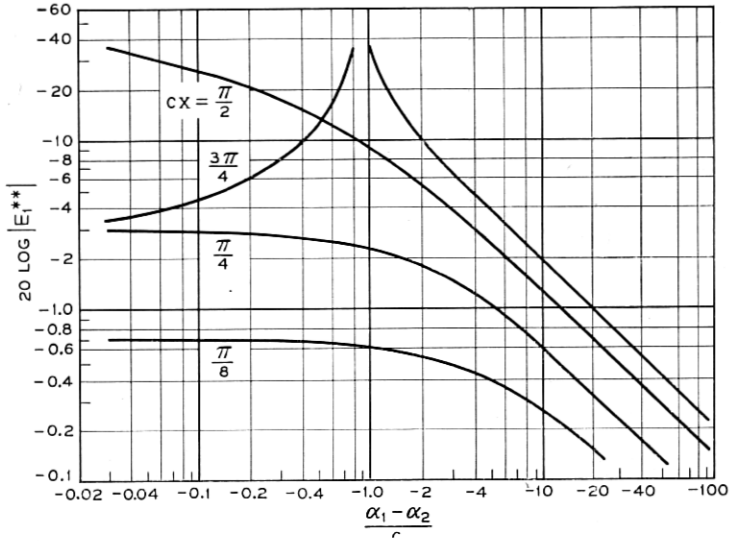

Fig. 21 — The effect of unequal attenuation constants on the driven line wave amplitude for equal phase constants, and $\underline{cx}$ constant. Negative $(\alpha_1 - \alpha_2)$ indicates that the undriven line has the larger attenuation constant.

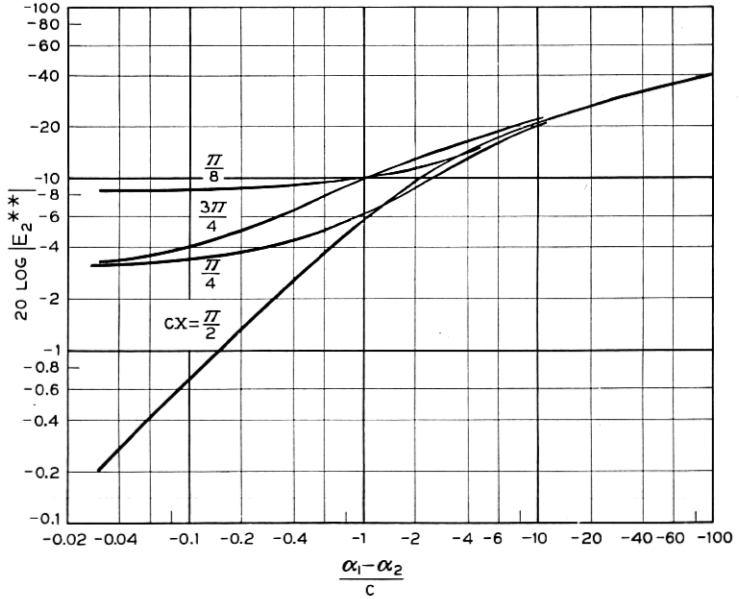

Fig. 22 — The effect of unequal attenuation constants on the undriven line wave amplitude for equal phase constants and $\underline{cx}$ constant.

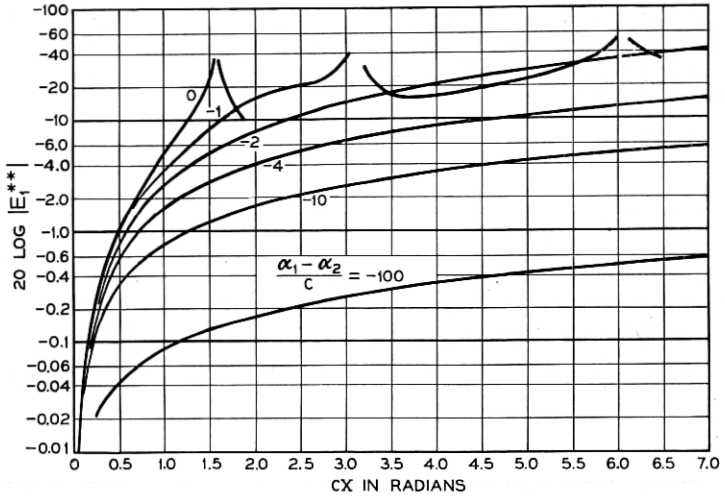

Fig. 23 — Driven line wave amplitude versus cx with equal phase constants and $(\alpha_1 - \alpha_2)/c$ as a parameter. The curve for $(\alpha_1 - \alpha_2)/c = 0$ is periodic.

For integrated coupling strengths greater than $\pi/2$ the effect of small values of $(\alpha_1 - \alpha_2)/c$ is to increase the loss to E_1**, as shown by the curve for $cx = 3\pi/4$ in Fig. 21. However, for sufficiently large values of $(\alpha_1 - \alpha_2)/c$ the loss to E_1** is made small.

The variation in E_1** and E_2** as a function of coupling strength (cx) is given in Figs. 23 and 24. The periodicity of E_1** is removed for

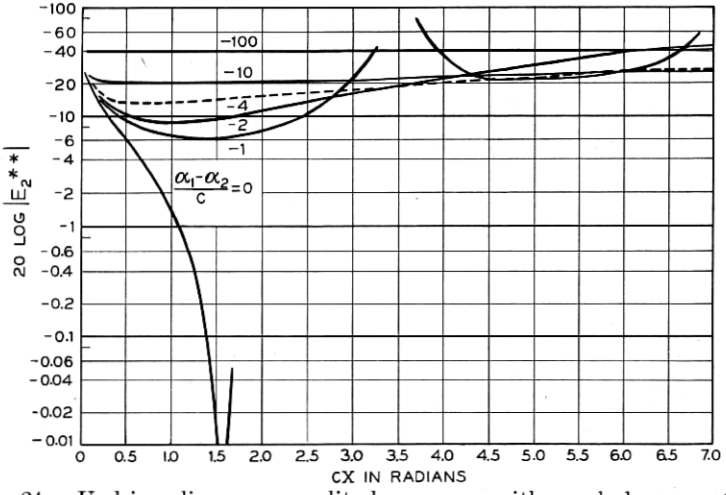

Fig. 24 — Undriven line wave amplitude versus cx with equal phase constants and $(\alpha_1 - \alpha_2)/c$ as a parameter. The curve for $(\alpha_1 - \alpha_2)/c = 0$ is periodic.

$(\alpha_1 - \alpha_2)/c$ as small as -1, but a value as large as -10 or more is required in order to reduce the loss to E_1^{**} to a moderate value for large integrated coupling ($\underline{c}x$) values.

When $(\alpha_1 - \alpha_2)$ is positive, the attenuation constant for the undriven line is less than that for the driven line, and under these circumstances E_1^{**} can exceed unity. Physically this means that the power loss line is carrying the energy for a distance and returning it to the driven line at a more distant point. The curves of Fig. 25 and Fig. 26 show the variation of E_1^{**} and E_2^{**} versus positive $(\alpha_1 - \alpha_2)/c$ values, at fixed values of integrated coupling strength $\underline{c}x$. For $\underline{c}x$ equal to $\pi/4$, the driven line wave magnitude E_1^{**} decreases as the ratio $(\alpha_1 - \alpha_2)/c$ assumes small positive values and goes through a balanced type of null near $(\alpha_1 - \alpha_2)/c = 3.5$ (see Fig. 25). Again this is the resultant of the lower loss undriven wave carrying power for a distance and returning it to the driven wave in the proper phase to cause cancellation of the straight-through component of the driven wave. For $\underline{c}x$ between $\pi/4$ and $\pi/2$ the null would move from $(\alpha_1 - \alpha_2)/c$ near 3.5 toward $(\alpha_1 - \alpha_2)/c = 0$.

Figures 27 and 28 show the variation of E_1^{**} and E_2^{**} versus the integrated coupling strength $\underline{c}x$ at fixed values of $(\alpha_1 - \alpha_2)/c$. In these

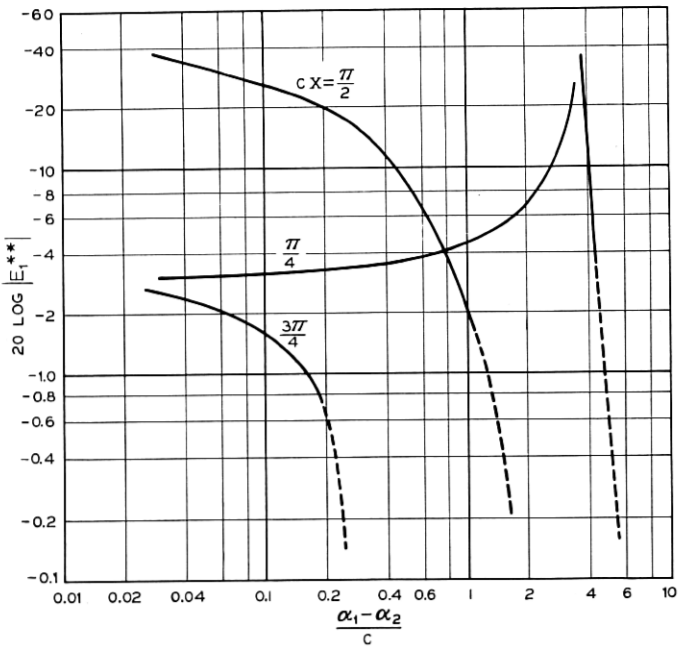

Fig. 25 — Driven line wave amplitude versus $(\alpha_1 - \alpha_2)/c$ with equal phase constants and $\underline{c}x$ constant. Positive $(\alpha_1 - \alpha_2)$ indicates the undriven line has the smaller attenuation constant.

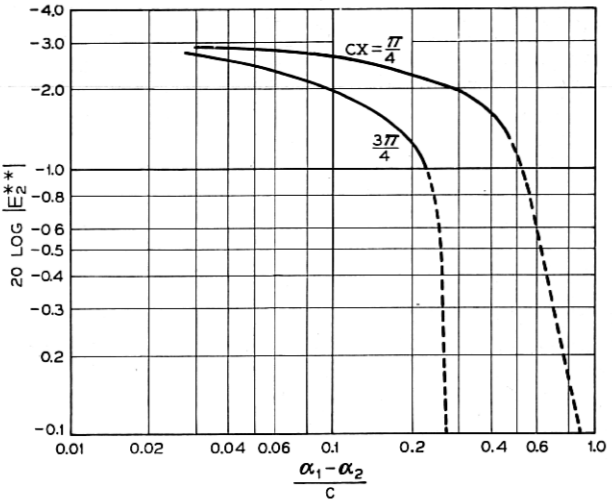

Fig. 26 — Undriven line wave amplitude versus $(\alpha_1 - \alpha_2)/c$ with equal phase constants and $\underline{cx}$ constant.

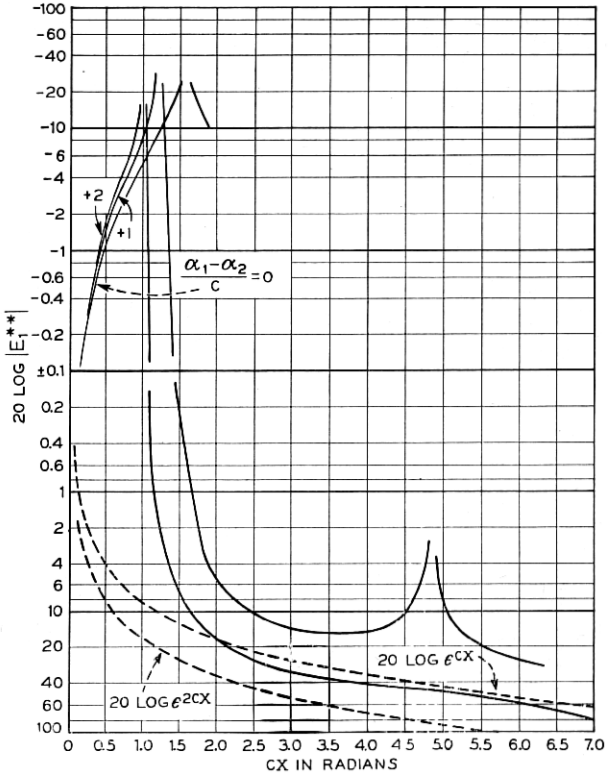

Fig. 27 — Driven line wave amplitude versus $\underline{cx}$, for equal phase constants; $(\alpha_1 - \alpha_2)/c$ as a parameter.

figures a double logarithmic scale is used on the ordinate to represent amplitude variations from 50 db below unity to amplitudes 50 db above unity. An arbitrary break in the scale has been made at ±0.1 db which for practical purposes will be assumed to correspond to amplitudes of unity. With reference to Figure 27, small positive values of $(\alpha_1 - \alpha_2)/c$ move the first null in E_1^{**} from $cx = \pi/2$ toward lower values of $c\underline{x}$. For abscissa values greater than $\pi/2$, E_1^{**} exceeds unity. For $(\alpha_1 - \alpha_2)/c = 1$, E_1^{**} again has a minimum in the vicinity of $cx = 3\pi/2$ but this second null has disappeared for $(\alpha_1 - \alpha_2)/c = +2$ and presumably also for larger positive values. With reference to Figure 28, E_2^{**} grows at a more rapid rate as a function of $c\underline{x}$ when $(\alpha_1 - \alpha_2)/c$ takes on positive values. The null in the vicinity of $cx = \pi$ is still present for $(\alpha_1 - \alpha_2)/c = 1$ but has disappeared at $(\alpha_1 - \alpha_2)/c = 2$. For $(\alpha_1 - \alpha_2)/c$ equal to +2 (and presumably for larger positive values) the undriven wave amplitude E_2^{**} is greater than E_1^{**} for $c\underline{x}$ larger than about 0.5.

The question comes to mind in connection with this case in which the

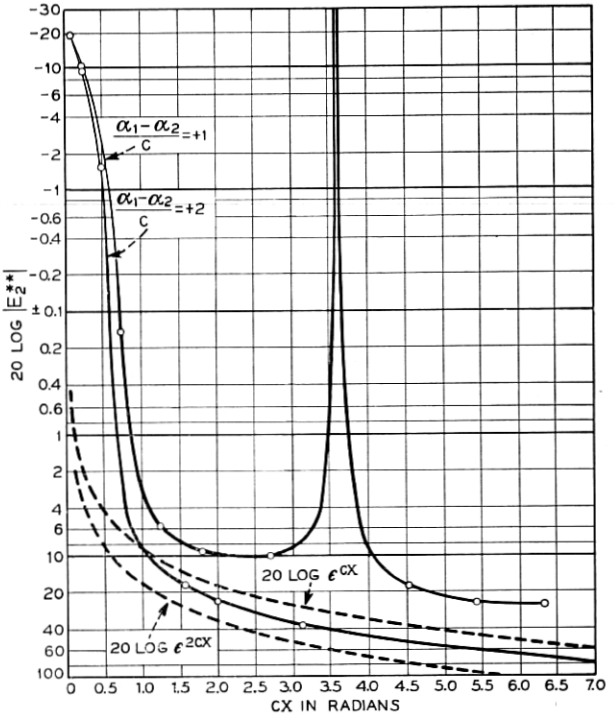

Fig. 28 — Undriven line wave amplitude versus $c\underline{x}$, for equal phase constants; $(\alpha_1 - \alpha_2)/c$ as a parameter.

undriven wave has a smaller attenuation coefficient than the driven wave, "How much less is the undriven line wave amplitude than would have existed at the same value of x if the same incident wave had been launched in the lower loss line and in the absence of coupling to the higher loss line?" This amplitude difference for the condition $(\alpha_1 - \alpha_2)/c = 1$ is represented in Fig. 28 by the *difference* between the curve for E_2** and the curve labeled 20 log e^{cx}. Similarly, for the condition $(\alpha_1 - \alpha_2)/c = 2$, this amplitude difference is represented by the difference between the curve for E_2** and the curve labeled 20 log e^{2cx}.

The general case of $\gamma_1 \neq \gamma_2$ is important both in interpreting undesired mode coupling effects in multi-mode systems as well as in evaluating

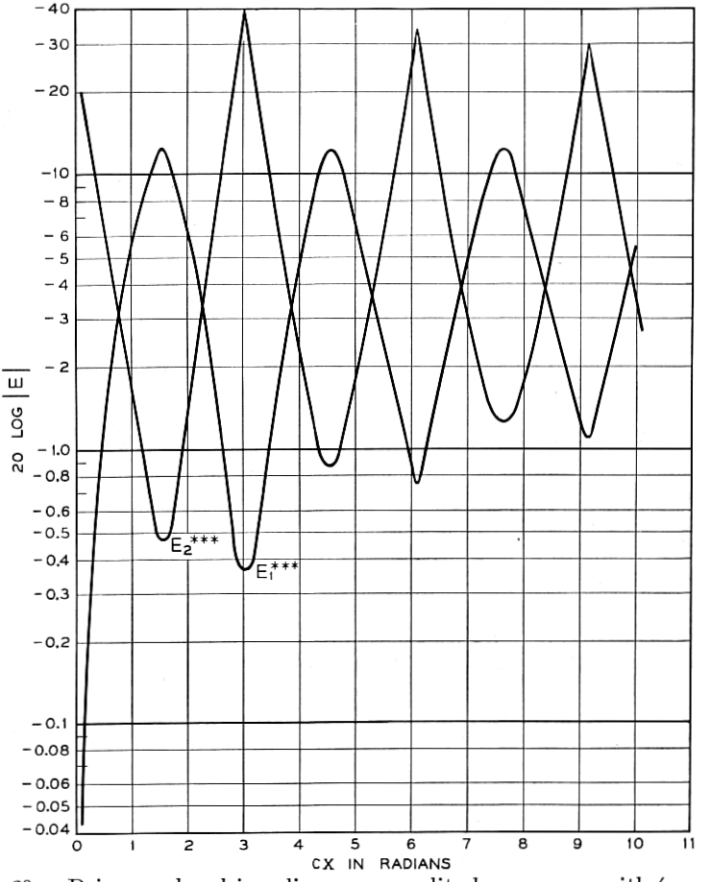

Fig. 29 — Driven and undriven line wave amplitudes versus cx with $(\alpha_1 - \alpha_2)/c = 0.03$ and $(\beta_1 - \beta_2)/c = 0.5$.

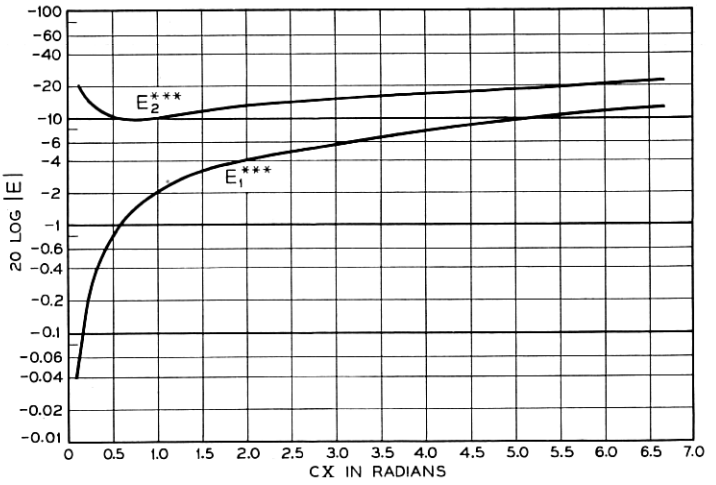

Fig. 30 — Driven and undriven line wave amplitudes versus $\underline{cx}$ with $(\alpha_1 - \alpha_2)/c = -2$ and $(\beta_1 - \beta_2)/c = 2$.

errors in construction of devices intended to produce $\gamma_1 = \gamma_2$. To facilitate discussion of this case we define

$$E_1 = E_1^{***}\epsilon^{-[\alpha_1 + i(c+(\beta_1+\beta_2)/2)]x}, \tag{37}$$

and

$$E_2 = E_2^{***}\epsilon^{-[\alpha_1 + i(c+(\beta_1+\beta_2)/2)]x}. \tag{38}$$

where E_1 and E_2 are defined by (21) through (24). The relation between E_1^{***} and E_1 (or E_2^{***} and E_2) is the same as described in connection with (35) and (36).

Small deviations from $\gamma_1 = \gamma_2$ are represented in Fig. 29, which shows E_1^{***} and E_2^{***} versus $\underline{cx}$ for $(\alpha_1 - \alpha_2)/c = -0.03$ and $(\beta_1 - \beta_2)/c = 0.5$. At $\underline{cx} = \pi/2$ radians, the first complete power transfer point in the $\gamma_1 = \gamma_2$ case, the above values correspond to a phase difference $(\beta_1 - \beta_2)x = \pi/4$ or 45°, and an attenuation difference $(\alpha_1 - \alpha_2)x = 0.03\ \pi/2$ or 0.047 nepers (0.41 db) for the path length of the coupling distance. In the absence of the dissipation difference, but for the same difference in phase constants, Fig. 20 shows that E_2^* reaches a maximum at −0.26 db near $\underline{cx} = \pi/2$, whereas the value including the dissipation difference (Fig. 32) is −0.46 db. The latter two values differ by 0.2 db or one-half of $(\alpha_1 - \alpha_2)x$; when $(\alpha_1 - \alpha_2)/c$ is small compared to unity, this is a general result.

More sizeable deviations from $\gamma_1 = \gamma_2$ are represented in Fig. 30, which shows E_1^{***} and E_2^{***} versus $\underline{cx}$ for $(\alpha_1 - \alpha_2)/c = -2$ and $(\beta_1 - \beta_2)/c =$

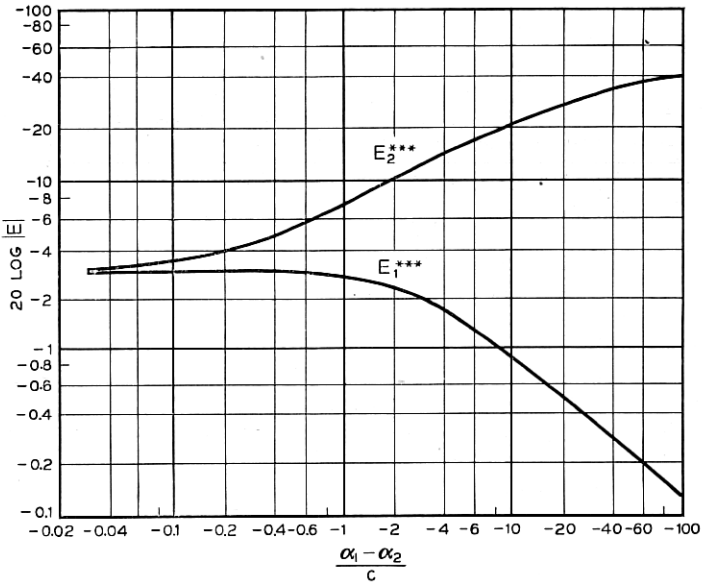

Fig. 31 — Driven and undriven line wave amplitudes versus $(\alpha_1 - \alpha_2)/c$ for $cx = \pi/2\sqrt{2}$ and $(\beta_1 - \beta_2)/c = 2$.

2. At $cx = \pi/2$, the phase difference is therefore π radians and the attenuation difference π nepers. The result is appreciable attenuation for E_1^{***} and only a moderate ratio of E_1^{***}/E_2^{***}.

Fig. 31 shows the way dissipation differences counteract the coupling forces when there is a phase constant difference $(\beta_1 - \beta_2)/c = 2$. This may be compared with Fig. 21 which represents the case of $(\beta_1 - \beta_2) = 0$. Very little change in E_1^{***} occurs until $(\alpha_1 - \alpha_2)/c$ exceeds $(\beta_1 - \beta_2)/c$; this is again a general result.

Finally, we may inquire as to how much power is dissipated in the system when attenuation constant differences are utilized to mitigate the effects of coupling. A measure of the power preserved is

$$| E_1^{***} |^2 + | E_2^{***} |^2$$

and this quantity is plotted in Fig. 32 for cases previously discussed in connection with Figs. 21 and 31. Either in the absence or presence of a phase constant difference, the attenuation constant difference shows a maximum effect in reducing the available power at $(\alpha_1 - \alpha_2)/c = 2$. This is probably a general result brought on by the factor

$$\sqrt{(\gamma_1 - \gamma_2)^2 - 4c^2}$$

found in the exponent of terms describing E_1 and E_2.

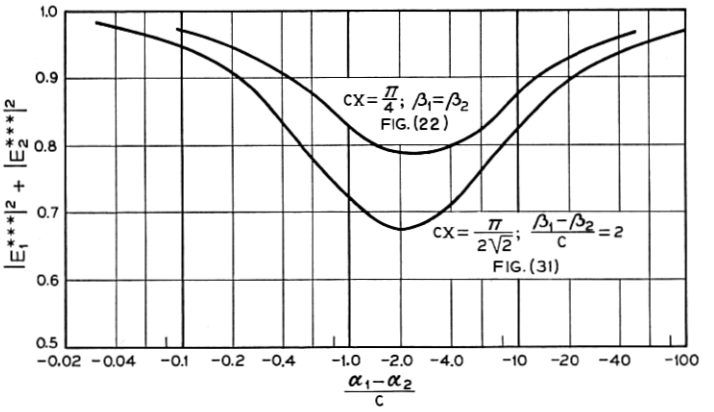

Fig. 32 — Available power versus $(\alpha_1 - \alpha_2)/c$ for several cases of interest.

TIGHT COUPLING EFFECTS OF MULTIPLE DISCRETE COUPLINGS

In practice it is convenient under some conditions to produce the desired coupling between transmission lines using multiple discrete couplings. It is then of interest to know the relation between the total power transferred and the number and strength of the individual couplings. It is the purpose of this section to state these relations.

We assume two transmission lines having identical propagation constants, with coupling units located at intervals along the lines as shown schematically in Fig. 33. A coupling unit may be a single point coupling, or an array of point couplings, but is always assumed to have the property of low reflection in the driven line and low back-wave transmission in the undriven line. If there are

n_1 couplings of magnitude α_1,

n_2 couplings of magnitude α_2,

and

n_k couplings of magnitude α_k

located along the lines in any order whatsoever, the wave amplitudes in

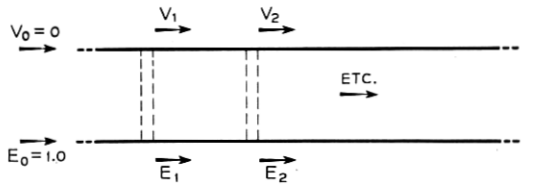

Fig. 33 — Schematic of transmission lines with multiple point couplings.

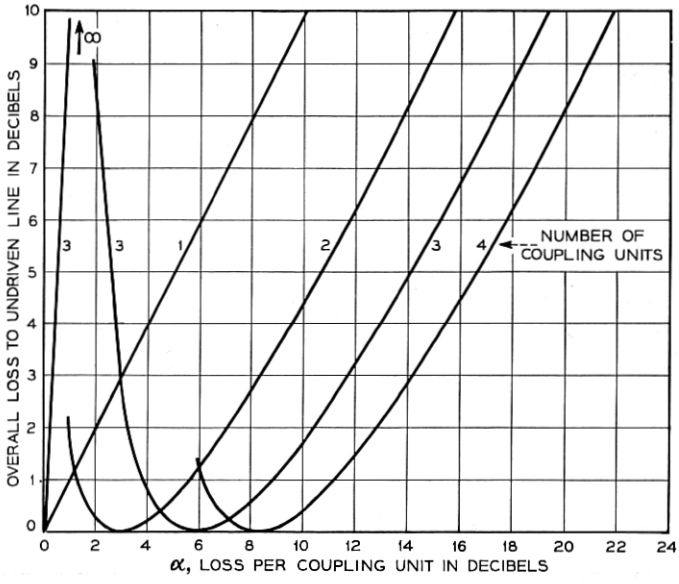

Fig. 34 — Overall loss to the undriven line versus loss per coupling unit, with the number of coupling units as a parameter.

the driven and undriven lines respectively are

$$E = \cos [n_1 \sin^{-1} a_1 + n_2 \sin^{-1} \alpha_2 + \cdots n_k \sin^{-1} \alpha_k], \qquad (39)$$

and

$$V = \sin [n_1 \sin^{-1} \alpha_1 + n_2 \sin^{-1} \alpha_2 + \cdots n_k \sin^{-1} \alpha_k]. \qquad (40)$$

These are amplitude factors due to coupling, and the normal attenuation effects in the uncoupled lines must be added separately. For complete power transfer we set the bracketed quantity of (39) and (40) equal to $\pi/2$, which gives the desired information about number and strength of point couplings. Other transfer losses may similarly be prescribed or determined.

For multiple coupling units of the same coupling strength, Fig. 34 shows the overall transfer loss to the undriven line versus loss per coupling units as a parameter. The shape of these curves from the complete transfer point toward higher losses is very nearly the same. Fig. 35 shows the loss per coupling unit versus number of coupling units, with overall transfer loss to the undriven line as a parameter.

SOME RESULTS OF EXPERIMENTS IN DOMINANT-MODE WAVEGUIDE

In a previous paper on dominant-mode waveguide directional couplers,[5] complete power transfer between dominant-mode rectangular

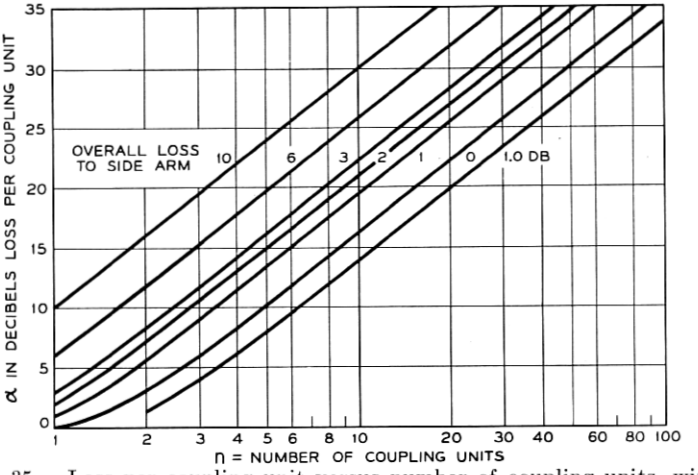

Fig. 35 — Loss per coupling unit versus number of coupling units, with the desired transfer loss as a parameter.

waveguides was shown to be possible in a coupling interval two wavelengths long, and very broad band directivity characteristics of a shape prescribed to meet given requirements were shown to be achievable.

The following paragraphs report on experiments which have been carried out with the objective of developing other useful devices and with the ancillary aim of verifying other predictions of the theory.

Experimental work was done to verify the cyclical nature of energy transfer between coupled lines, to determine the magnitude of losses which accompany such transfer in the waveguide case, and to determine desirable coupling distribution shapes in the tight coupling case. These experiments were carried out by R. W. Dawson in the 3.1 to 3.5 cm band using the 0.4″ x 0.9″ I.D. jig shown in Fig. 36, consisting of two wave-

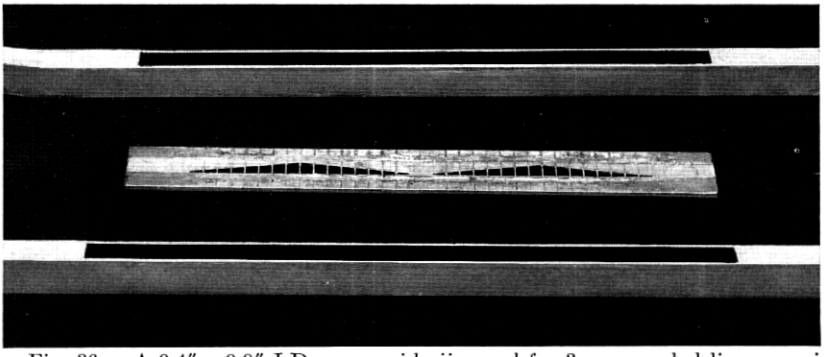

Fig. 36 — A 0.4″ x 0.9″ I.D. waveguide jig used for 3 cm coupled line experiments. The long waveguides on one side of the coupling insert were required to accommodate low-reflection terminations for directivity measurements.

guides having one wall cut away to accept a coupling insert. In one set of observations, the insertion loss in the driven-line and the transfer loss to the undriven line were recorded for a variable number of No. 22 copper wires dividing a coupling aperture $11\frac{1}{4}''$ long and linearly tapered from 0.030″ height at the ends to 0.33″ height at the center. The results are recorded in Fig. 37. At 102 holes, negligible power was abstracted from the driven line, and the transfer loss to the undriven line forward wave $|E_2|$ was about 18 db. Note that more coupling was observed at

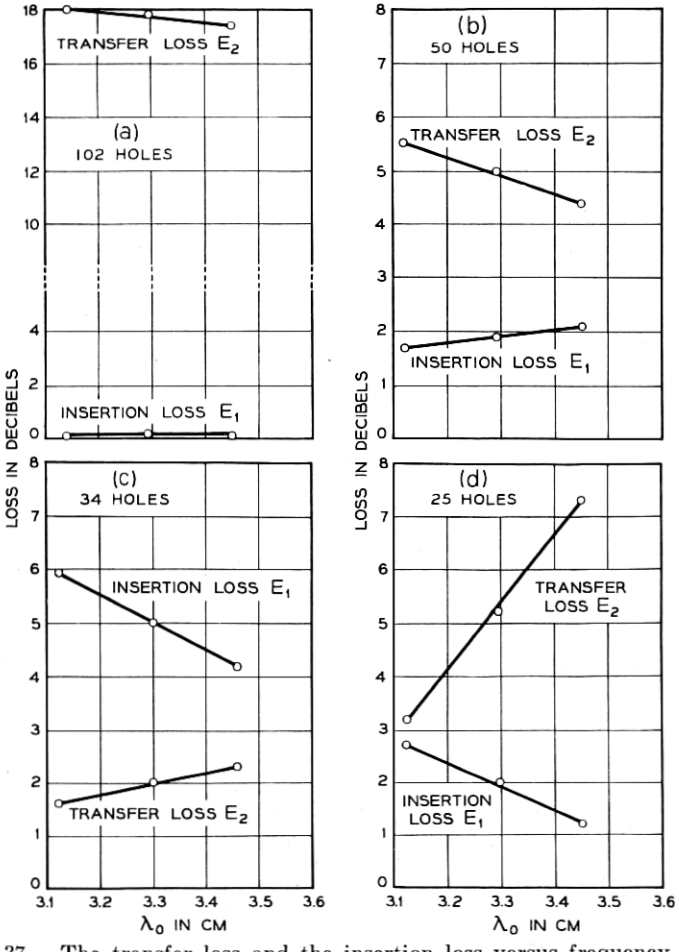

Fig. 37 — The transfer loss and the insertion loss versus frequency for the coupled waveguides of Fig. 36, showing the cyclical exchange of power as the coupling was increased by reducing the number of dividing wires in the fixed coupling aperture.

increasing wavelength values, a general result for small holes in the side wall. As the number of wires in the given aperture was reduced, markedly increased coupling resulted. This was due to the fact that the coupling loss per hole varied approximately as the fourth power of the hole dimension perpendicular to the electric vector, whereas the overall power loss varied only as the square of the number of holes in the loose coupling region. (Equations (39) and (40) describe the effects of number of coupling points more precisely.) At 50 holes, the transfer loss was about 5 db and the wave in the driven line was reduced by about 2 db; the slope of the $|E_2|$ versus λ_0 plot was the same as for 102 holes. At 34 holes, the transfer loss was about 2 db and the wave in the driven line was reduced by about 5 db; in this case, however, the undriven line wave loss increased with increasing λ_0. Since coupling increases with increasing λ_0 we deduced that the total coupling was greater than required for complete power transfer and the bracketed expression of (39) and (40) was greater than $\pi/2$. On the diagram of Fig. 16, the presumed operating point was near $cx = 2.2$ radians. At 25 holes, Fig. 37(d), the transfer loss was about 5 db and the wave in the driven line was reduced by about 2 db; as in the 34 hole case, the undriven line wave amplitude decreased with increasing λ_0 and hence with increasing coupling. Again the integrated coupling appeared to be in the region between $\pi/2$ and π. The driven line wave loss was headed for a low value at the long-wave end of Fig. 37(d), and it seems clear that periodic energy exchange is realized in practice.

The losses associated with this energy exchange may be inferred by comparing the total power output of the undriven and driven lines to the input power. Assuming that the forward waves in the driven and undriven lines contain all the output power, (i.e. neglecting reflection, back wave in the undriven line and waveguide losses) the following table gives the losses observed in the above described experiments:

Number of Holes	Coupling Mechanism Loss
	db
50	0.16
34	0.23
25	0.33

These losses may be due to circulating currents in the wires, in which case the loss would be expected to increase with increasing coupling.

Good agreement between the observed and theoretical directivities has been found in the loose coupling case,[5] but when appreciable power is

abstracted from the driven line it is clear that the theory given above does not apply. Dawson has obtained experimental data of interest in this connection. For a $6\lambda_g$ long linear-taper aperture of the form given above (0.33″ height at the center and 0.030″ height at the ends), the loose coupling theory predicts directivities in excess of 45 db for the wavelength band 3.1 to 3.5 cm. When using sufficient number of wires to obtain 18 db transfer loss, directivities in the range 36 to 48 db were observed. The reason for the 36 db observation being lower than the 45 db theoretical value may be inaccuracy of fabrication (jig per Fig. 36) or inapplicability of the loose coupling theory at 18 db transfer loss. At 3 db transfer loss, the observed directivity of a similarly shaped but 5.5 λ_g long coupling array is shown at the top of Fig. 38; again loose coupling theory predicts more than 45 db directivity. The reason the observed values are in the 24–33 db range rather than above 45 db is presumed to

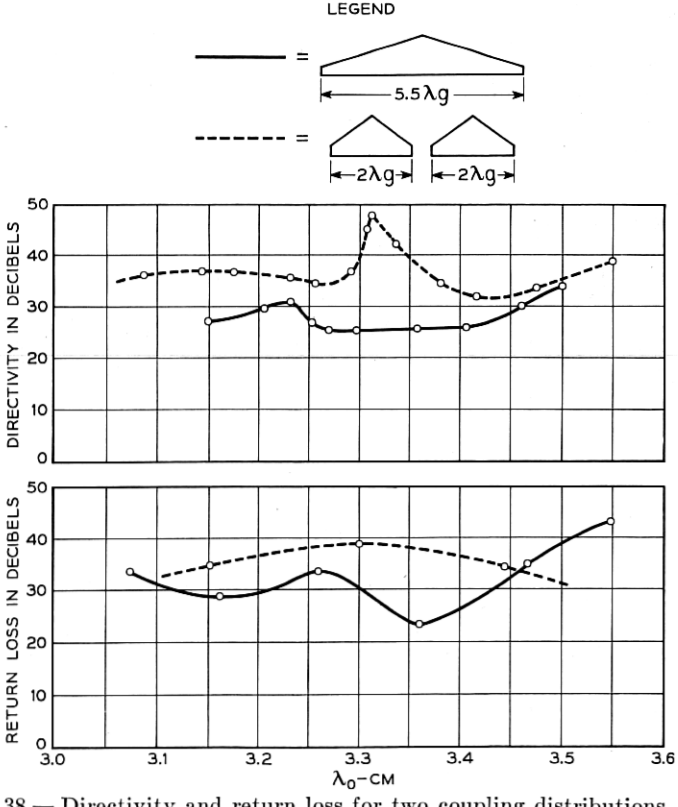

Fig. 38 — Directivity and return loss for two coupling distributions, each of which produced 3 db transfer loss.

TABLE I

Array	Transfer Loss		
	λ_0 = 3.15 cm	λ_0 = 3.30 cm	λ_0 = 3.45 cm
	db	db	db
Single $2\lambda_g$ array	3.2	3.0	2.8
Two cascaded arrays	4.3	4.2	4.0
Single $5.5\lambda_g$ array	3.5	2.9	2.4
Array	Straight Through Loss		
	λ_0 = 3.15 cm	λ_0 = 3.30 cm	λ_0 = 3.45 cm
	db	db	db
Single $2\lambda_g$ array	3.0	3.2	3.5
Two cascaded arrays	2.6	2.8	3.0
Single 5.5 λ_g array	2.9	3.6	4.3

be inapplicability of the theory. Loose coupling theory predicts better than 35 db directivity over a broad frequency band at a coupling length of about $2\lambda_g$; therefore one might expect to obtain better overall results by using two cascaded arrays each about $2\lambda_g$ long, and each having a transfer loss of 8.4 db to get the 3 db net transfer loss. Observed directivities for such a coupling array are also given in the top of Fig. 38; in this case values in the 32–37 db region were obtained. The destructive interference associated with addition of backward wave components is more nearly of the form computed by loose coupling theory because the exciting wave is more nearly constant over the length of one of the arrays. The observed return loss at any one of the four waveguide entries, when the others are terminated, is given for the $5.5\lambda_g$ and cascaded $2\lambda_g$ coupling arrays at the bottom of Fig. 38. The cascaded $2\lambda_g$ combination is again superior to the single long taper. The characteristic of being inherently matched at all terminals makes the coupled-line type of 3 db hybrid attractive at the very high frequencies where lumped element matching becomes difficult if not impracticable.

Where space is at a premium, or where more constant transfer loss values are to be desired a shorter array composed of larger holes is attractive. A single linear taper of the shape outlined above and $2\lambda_g$ long was observed to have better than 22 db directivity and better than 25 db return loss over the 3.1 to 3.5 cm band. The observed loss values of the three coupling arrays discussed above are given in Table I. The coupling arrays composed of larger holes have less slope in the loss versus frequency characteristic for side-wall coupling.

SOME LOOSELY COUPLED TRANSDUCERS IN MULTIMODE WAVEGUIDE

In connection with research on low-loss circular-electric-wave transmission,[1] there developed a need for means with which to measure the power present in any one of the modes of a multi-mode round waveguide. In particular, it was known that the circular electric wave in round waveguide converts readily to the TM_{11} wave due to curvature of the line,[2] and a direct measurement of the effect was needed. The TM_{11} wave will not exist in the round waveguide without the presence of at least four other modes, and in the waveguide size used for the experiments five other modes could propagate. In designing a transducer for this application, therefore, it was necessary to evaluate the discrimination function, equation (4), with regard to mode discrimination between five different pairs of modes as well as to insure directivity. Moreover, the TM_{11} wave is degenerate with the circular electric wave TE_{01}, i.e., they have the same phase constant. Therefore, mode discrimination against TE_{01} could not be obtained through the phase difference effects described by (4). This discrimination was obtained using geometric balance in the individual coupling orifices, which were narrow slits on the center line of the wide side of the rectangular guide, as shown in Fig. 39. The shape of the coupling distribution employed was that described in connection with Fig. 14 except that 80 point couplings were used to simulate the raised-cosine coupling distribution (instead of 40 as in Fig. 14) in order to assure good directivity for the very long coupling length that was required. The round guide diameter was two inches, the rectangular guide width 0.820 inches, calculated to produce the same cut-off frequency in the rectangular guide as exists for the TM_{11} wave in the round waveguide. The coupling length was about 17 inches.

One simple method for evaluating the mode content of such a transducer is to measure the azimuthal distribution of electric field at the round guide wall using the radial probe technique described by M. Aronoff.[7] If the power in a single mode is a great deal larger than the

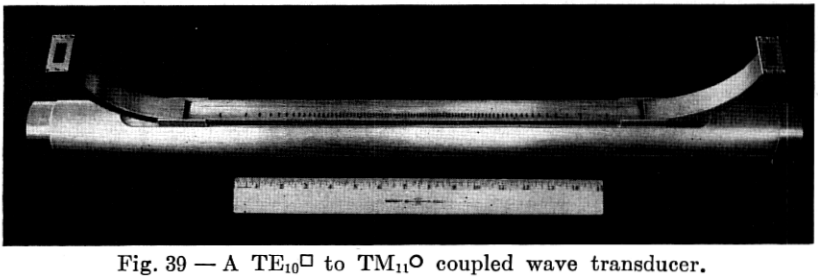

Fig. 39 — A TE_{10}□ to TM_{11}○ coupled wave transducer.

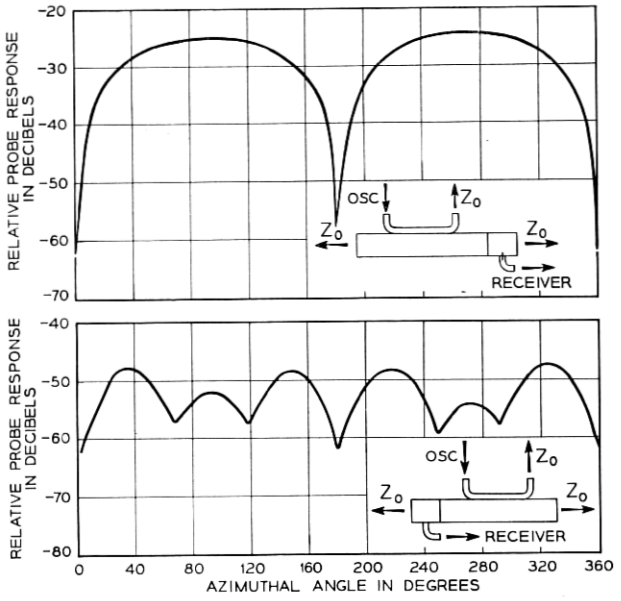

Fig. 40 — Distribution of radial electric field at the guide wall for the forward and backward waves of the transducer of Fig. 39.

power in any other mode of the multi-mode guide, the radial probe technique narrows down the possible mode types to a very few. Measurements of this type, recorded in Fig. 40, indicate that the forward wave has the radial electric field distribution to be expected for the TM_{11} wave. However, the forward wave might have the same radial field distribution at the wall and actually be the TE_{11} wave instead of TM_{11}. The TE_{11} wave is very simply generated from a dominant mode rectangular guide, by means of a long taper transition along the axis of propagation from the rectangular cross section to the circular cross section. Such a transducer was used to measure the output wave of the TM_{11} transducer and it was found that the TE_{11} component was down on the order of 30 db below the value which would be present if the radial field intensity observed at the top of Fig. 40 had been due to TE_{11}. By a process of elimination, therefore, and by virtue of the fact that we have a pure pattern suggesting the presence of a single mode, we have established that the mode generated is actually TM_{11}. Other checks can of course be made, such as measurement of the phase constant of the output wave.

The backward wave shown at the bottom of Fig. 40 has a maximum field more than 20 db below the maximum field of the forward wave and

has a six-peaked variation with angle which indicates the presence of TE_{31}.

The transfer loss of the TM_{11} transducer was derived by (1) calibrating the receiving probe on a known amount of power in the TE_{11} wave, (2) inserting this same amount of power in the rectangular waveguide of the coupled wave transducer and, with the probe at the transducer output, observing the change in the receiver response, and (3) correcting the observed loss using the theoretical difference in the radial electric field at the wall for the TE_{11} versus TM_{11} waves in the known waveguide diameter. (This technique is described in more detail by Aronoff.[7]) The result gave a transfer loss of about 25 db to the TM_{11} wave. The insertion loss for the rectangular guide of the transducer was less than 0.2 db.

Coupled-wave devices of the type shown in Fig. 39 were built for several of the modes in 2″ round waveguide. The one built for the TE_{31} mode in 2″ waveguide (mechanically similar to the TM_{11} model of Fig. 39) has several characteristics worthy of mention. Fig. 41 shows the

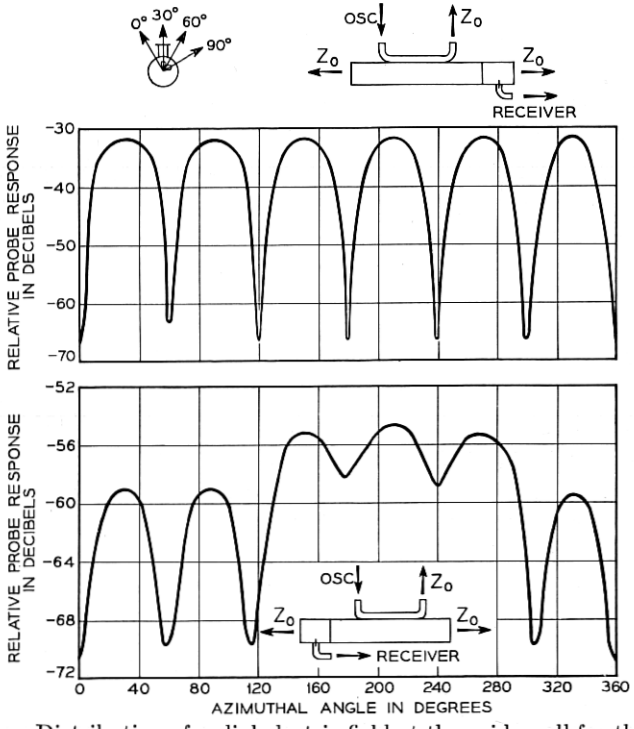

Fig. 41 — Distribution of radial electric field at the guide wall for the forward and backward waves of TE_{10}□ to TE_{31}○ coupled wave transducer.

TABLE II

Ratio of Forward Traveling TM_{11} Power to	Observed Discriminations		
	λ_0 = 3.1 cm	λ_0 = 3.3 cm	λ_0 = 3.5 cm
	db	db	db
TM_{11} Backward	>20	>20	>20
TE_{11} Forward	28.5	28	26
TE_{11} Backward	37	35	39
TM_{01} Forward	46	46	41.5
TM_{01} Backward	49	51	45.5
TE_{21} Forward	24.5	21	23
TE_{21} Backward	29.5	35	31
TE_{31} Forward	14	26	21.5
TE_{01} Forward	45	46	45
TE_{01} Backward	64	69	67

measured forward and backward wave patterns in the round guide, for excitation in one of the rectangular guides of the transducer. Only TE_{31} of the six modes possible in the 2″ pipe at 3.3 cm has a six-lobed pattern of azimuthal distribution of radial electric field at the wall, and hence the clean pattern with equally spaced deep nulls indicates the presence of a rather pure TE_{31} mode. The six maxima of the forward wave were equal within ±0.15 db. The backward wave had a peak electric field at least 23 db down on the peak electric field of the forward wave.

Using coupled transmission line techniques and the familiar geometric taper techniques, transducers were built for all of the six modes possible in 2″ diameter pipe at 3.3 cm for use in the circular electric wave research program.[1] These transducers were used to measure the forward wave and backward wave output of the TM_{11} transducers, as given is Table II. In reality, imperfections in either one of the two transducers involved in a measurement could result in the recorded values of discrimination. For example, if the TM_{11} transducer were perfect and the TE_{01} output transducer contained some TM_{11} . then the insertion loss measurement involving the two transducers face to face would produce an indication of mode impurity. Since we do not have independent information on the mode purity of any one of the transducers at the level of the observed wave impurities, we can only state that both transducers involved in a discrimination measurement are probably at least as good as the number tabulated.

It should be noted that very high discriminations between TE_{01} and TM_{11} were achieved, despite the fact that this one discrimination depends solely on the mode-selective nature of the coupling orifice. Similar discriminations can be employed effectively to augment the wave-inter-

ference discrimination even in cases where there is difference between the desired and undesired modes' phase constants, to achieve very large discriminations. In the TM_{11} discriminations listed above, the values for TE_{31} are not great but are consistent with computed values for the coupling length and the coupling function employed; longer coupling lengths would produce better TM_{11} versus TE_{31} discriminations.

A TIGHTLY COUPLED $TE_{10}^{\square}$ TO TE_{01}° WAVE TRANSDUCER*

A highly efficient means of transferring power from dominant-mode rectangular waveguide to one of the higher modes of a multi-mode waveguide would be essential in a waveguide transmission system.[1] When several modes can propagate in one or both of the guides, the problem of achieving complete power transfer is more difficult and requires some new techniques. This section describes these techniques and gives experimental data for a circular-electric-wave ($TE_{10}^{\square} - TE_{01}^{\circ}$) transducer.

The desired transducer was required to make the wave transformation between a single-mode rectangular waveguide and the circular electric mode (TE_{01}°) of an 0.875″ round waveguide at a nominal frequency of 24,000 mc. The 0.875″ round waveguide at this frequency will support 10 modes of which the circular electric mode and its degenerate partner TM_{11}° are the fourth and fifth in order of appearance.

The minimum length of the coupling interval required to achieve mode discrimination may be estimated using loose coupling theory (equation 4). The mode nearest to TE_{01}° in phase constant is the TE_{31}° and for this mode a coupling length of about 0.18 meters is required in order to produce a value of θ/π equal to unity. As shown by equation (5) for uniform coupling, it is necessary to have θ/π equal to unity or greater in order to develop discrimination against the undesired mode.

The maximum coupling coefficient permissible for a given amount of mode impurity at the complete power transfer point may be estimated using the tight coupling theory of the preceding sections. For example, equations (31) and (32) show that for the ratio $(\beta_1 - \beta_2)/c$ equal to 10, the transfer loss to the undesired wave will always be greater than 14 db (regardless of the length of the coupling interval), corresponding to an energy loss for the desired wave of less than 0.2 db. For the TE_{01}° and TE_{31}° modes the calculated values of β_1 and β_2 lead to the conclusion that the coupling coefficient c between TE_{31}° and $TE_{10}^{\square}$ must be less

* When discussing the modes of hollow metallic waveguides of different cross-sectional shapes, it has been found convenient to use a superscript to designate the shape of the cross section. (See G. C. Southworth, *Principles and Applications of Waveguide Transmission*, D. Van Nostrand Co., 1950). Thus, $TE_{10}^{\square}$ refers to the TF_{10} mode in rectangular waveguide.

than 3.45 radians per meter. If the coupling coefficient for $TE_{10}^{\square}$ to TE_{01}° is equal to that for $TE_{10}^{\square}$ to TE_{31}° it follows that the total coupling length must be greater than 0.455 meters, because complete power transfer requires that the product of coupling-length times coupling-coefficient be exactly $\pi/2$ (see Fig. 17). Actually, the $TE_{10}^{\square} - TE_{31}^{\circ}$ coupling may be greater than the $TE_{10}^{\square} - TE_{31}^{\circ}$ coupling which leads to the requirement for longer coupling intervals. It is evident that the shorter coupling intervals may be employed at the sacrifice of greater mode impurities. The preceding calculations were made for the $TE_{10}^{\square} - TE_{31}^{\circ}$ and $TE_{10}^{\square} - TE_{01}^{\circ}$ transfer ratios as though only one mode of the multi-mode waveguide were present at a time, i.e., using a theory based on coupling between two waves instead of a theory for the simultaneous coupling between a plurality of waves. It is felt that this is probably

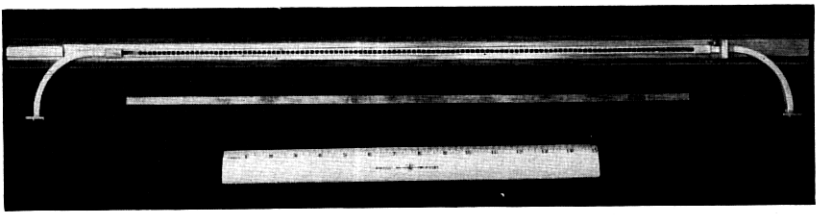

Fig. 42 — An experimental circular electric wave ($TE_{10}^{\square}$ to TE_{01}°) transducer for 24,000 mc.

justified provided that the coupling per unit length is weak and only one mode in each guide carries an appreciable amount of power.

Fig. 42 shows a photograph of one of the models used to obtain experimental data. The coupling holes were located in the narrow wall of the rectangular waveguide, thus avoiding coupling to all of the TM modes of the round waveguide. The total coupling length was 0.55 meters. The coupling orifices were spaced about 0.3 wavelengths in the dominant-mode rectangular waveguide, which assured reasonable directivity in the transfer of power between waveguides, provided that two or more coupling elements were employed.

The transfer loss between the rectangular waveguide and the circular electric mode of the round waveguide was measured as a function of the number of coupling elements, using the structure of Fig. 42 with the addition of a movable thin-walled metallic cylinder. The latter could be moved inside the transducer in such a way as to cover up a variable number of coupling holes, and contained a long wooden termination so that all the power entering the movable cylinder was absorbed. The inner diameter of the movable cylinder was large enough to propagate the

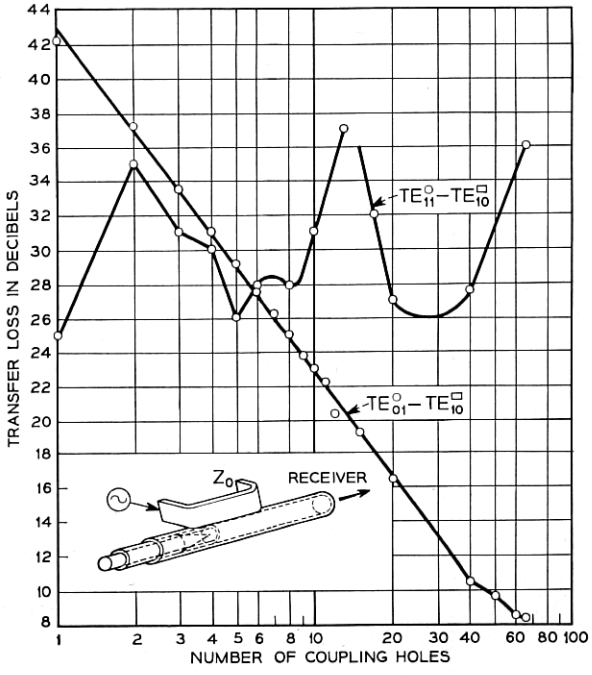

Fig. 43 — Transfer losses versus frequency for the transducer of Fig. 42.

circular electric wave but did cut off some of the waves which could propagate in the round guide of the transducer itself. The measured transfer loss under these conditions is recorded in Fig. 43. It is seen that the $TE_{10}^{\square}$ — TE_{01}° coupling was so weak as to be in the region where power from successive coupling elements should add inphase all the way up to 40 coupling elements. The observations show the inphase addition for less than 30 coupling elements but show a marked deviation in the vicinity of 40 to 66 coupling elements. This is evidence of inequality of the phase constants for the TE_{01}° and $TE_{10}^{\square}$ waves. More will be said about this matter presently. The transfer loss between the rectangular waveguide and the TE_{11} mode of round waveguide, is also recorded in Fig. 43. As expected, the power from successive coupling elements did not add inphase and no appreciable build-up of power in the TE_{11} mode took place.

One way of evaluating the total power in all modes other than the circular electric mode, is to measure the value of the transverse magnetic intensity at the wall of the round waveguide. The circular electric wave has no such field component and all other waves do possess such a field

component. Thus the total value of the transverse magnetic intensity at the round waveguide wall is a measure of the impurity associated with the circular electric wave. (This is very similar to the radial probe technique described by M. Aronoff.[7]) Using this method of evaluation, the mode impurities present at the output of the transducer were measured as a function of the number of coupling elements, and the results are recorded in Fig. 44. The absolute calibration of the ordinate relates the observed magnetic intensity to that which the same power input used at the rectangular guide would have produced if placed in the round waveguide in the TE_{11} mode. These measurements show that for all of the modes other than the circular electric mode, the energy components from successive coupling elements suffer destructive interference. Although curves are shown only for one and for 66 coupling elements, the patterns for intervening numbers of coupling elements were similar in shape and never exceeded an intensity value greater than about 6 db above that given for the 66 coupling element case; thus the mode discriminating property of the coupled wave transducer was verified experimentally.

Returning to the question of $TE_{10}^{\square} - TE_{01}^{\circ}$ transfer loss, it is clear from Fig. 43 that the rectangular waveguide has a phase constant which is not equal to that of the circular electric mode in the round waveguide. One reason for this inequality lies in the fact that the coupling elements disturb the phase constant in the two waveguides unequally, a consequence of the fact that some of the power transferred to the round wave-

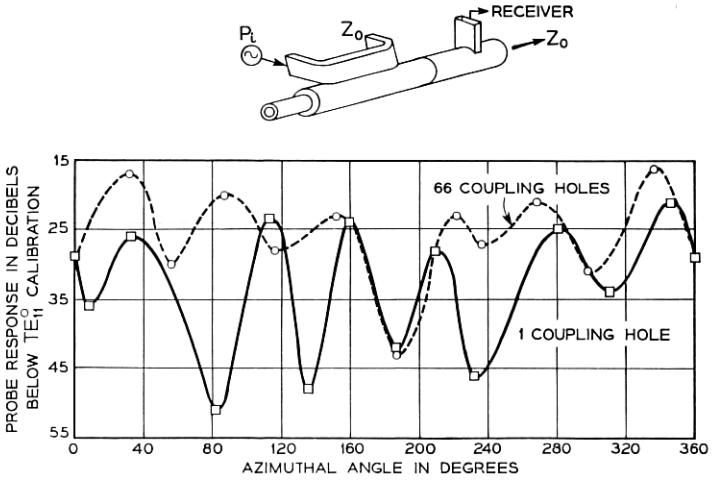

Fig. 44 — Distribution of transverse magnetic intensity at the wall for the transducer of Fig. 42.

guide on a single coupling element basis, appears in modes other than TE_{01}. Thus, the total coupling to $TE_{10}^{\square}$ is greater than to TE_{01}°. The total coupling modifies the phase constant of each line, per (20′), and since the total coupling coefficient is unequal for the $TE_{10}^{\square}$ and the TE_{01}° modes, the perturbed phase constants should be expected to be unequal when the unperturbed phase constants are made equal. A method of determining the magnitude of this phase-constant disturbance has been suggested by S. A. Schelkunoff. In this method the reflected wave from a single coupling orifice is measured in the dominant waveguide and in the single mode of interest in the multi-mode waveguide. Having defined the ratio of the incident to the reflected power in the same mode by the sympol p, Schelkunoff determines that the disturbed phase constant β', is related to the undisturbed phase constant β by the relation

$$\beta' = \beta + \sqrt{\frac{p}{d}}, \tag{41}$$

in which "d" is the distance between the coupling orifices in the coupling arrangement which one wishes to evaluate. This relation may be used to evaluate the change in the phase constant for the circular electric mode and for the wave in the dominant waveguide, and the change of wave-

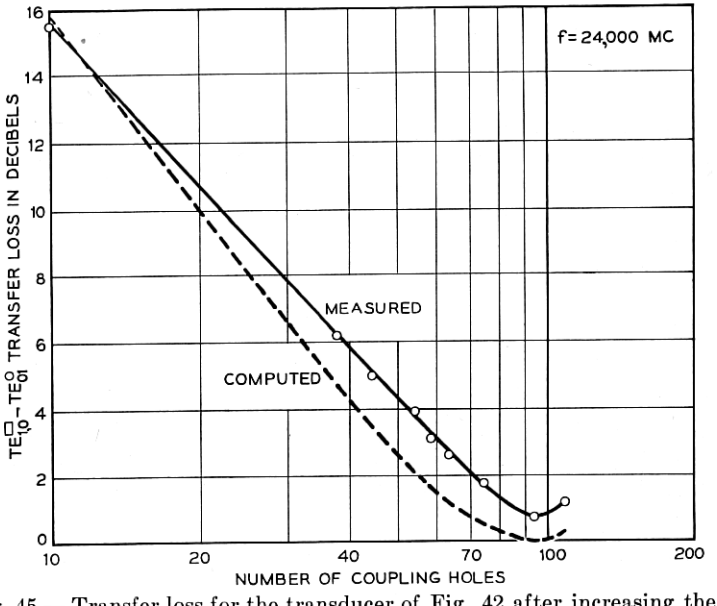

Fig. 45 — Transfer loss for the transducer of Fig. 42 after increasing the coupling hole sizes and correcting the phase constant.

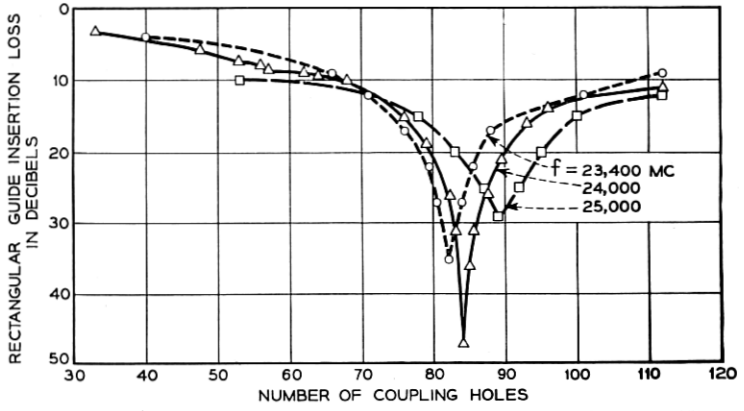

Fig. 46 — Rectangular guide insertion loss for the transducer of Fig. 42.

guide dimensions required to correct this phase constant difference may be computed as though the coupling elements were not present.

For the small phase constant disturbances which are associated with the weak couplings employed, this procedure was found very accurate. The reflection measurements and associated calculations for the model of Fig. 42 indicated that the rectangular guide width should be 0.340″ for equality of phase constants instead of 0.359″ as computed neglecting coupling effects. The measured value of the transfer loss when the individual coupling holes had been enlarged and the rectangular guide width had been altered to the 0.340″ value is shown in Fig. 45. It is evident that the theoretical value of 0 db transfer loss was approached, and that the shape of the transfer loss versus number of coupling elements, was reproduced very well. The 0.75 db minimum transfer loss consisted of no more than 0.3 db heat loss, the remaining loss being due to power present in other modes.

The measured insertion loss in the rectangular waveguide is shown as a function of the number of coupling holes at the three frequencies in Fig. 46. Complete power transfer would, of course, correspond to an infinite insertion loss in the rectangular waveguide. It is interesting to note that at 24,000 mc the peak in the rectangular guide insertion loss occurred at 85 coupling elements whereas the maximum in the $TE_{10}^{\square} - TE_{01}^{\circ}$ transfer loss characteristic occurred at about 96 coupling elements (Fig. 45). This difference is likely to be the result of power transferred back to the rectangular waveguide from round waveguide modes other than circular electric. Additional evidence of deviations due to the coupling between a plurality of waves was obtained; the rectangular-guide insertion loss as a function of number of coupling elements did not increase

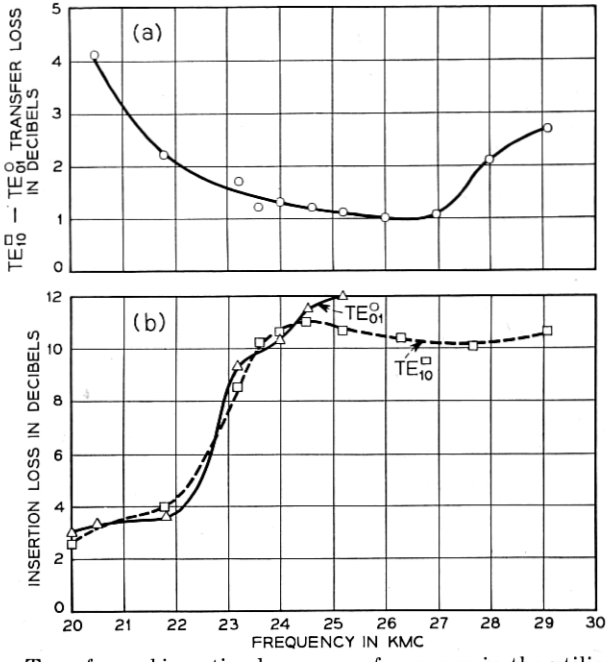

Fig. 47 — Transfer and insertion loss versus frequency in the utilized modes of the transducer of Fig. 42 using all (112) coupling holes.

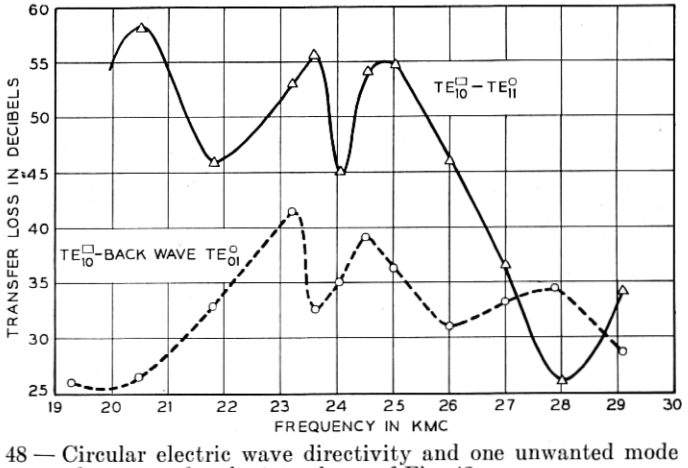

Fig. 48 — Circular electric wave directivity and one unwanted mode (TE_{11}° output versus frequency for the transducer of Fig. 42.

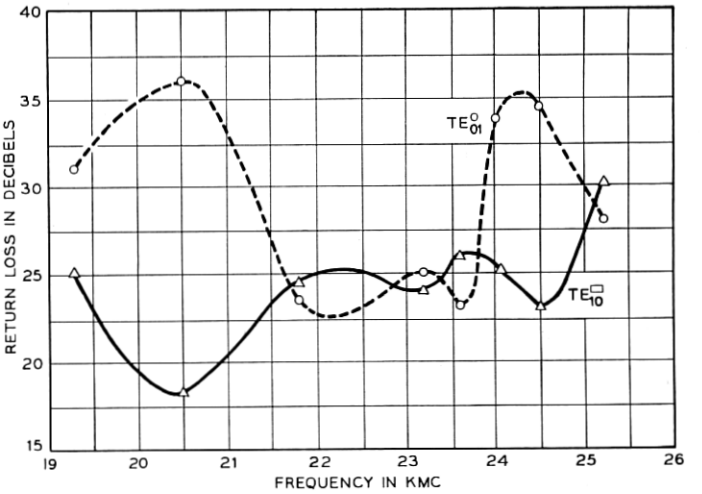

Fig. 49 — Impedance characteristic of the transducer of Fig. 42.

smoothly according to a cosine amplitude function as would be expected for two coupled waves of identical phase constant, but instead exhibited ripples. The remarkable thing about the data of Figs. 45 and 46 is that it agrees with the theory for two coupled waves as well as it does.

The coupling per individual orifice decreases with increasing frequency and this is verified by the observation (Fig. 46) that a greater number of coupling elements are required to reach the maximum insertion loss in the rectangular guide at the higher frequency.

Some indication of the overall bandwidth of this first experimental model is given in Figs. 47, 48 and 49 which show respectively the $TE_{10}^{\square}$ – TE_{01}° transfer loss, the insertion losses in the $TE_{10}^{\square}$ and TE_{01}° modes, the $TE_{10}^{\square}$ – TE_{11}° and $TE_{10}^{\square}$ – backward wave TE_{01}° transfer losses, and the $TE_{10}^{\square}$ and TE_{01}° return losses in the frequency range 20,000 to 30,000 mc. No one of these characteristics represents the degree of excellence which is achievable but they do demonstrate that good impedance match, low transfer losses to the desired mode, and appreciable discrimination against unwanted modes, can be achieved over frequency ratios on the order of 1.5.

FREQUENCY SELECTIVITY

In the case wherein the coupling is so weak as to not affect the total phase constant appreciably, all modes of hollow conductor waveguides of any cross section have the same phase constant at all frequencies provided that these modes have the same cut-off frequency. This results

in very broad band mode-selective characteristics, as has been demonstrated.

The transfer loss characteristics are in general a function of frequency, since the individual coupling holes are somewhat frequency selective. There may be applications wherein less variation in transfer loss as a function of frequency is required. One approach to this problem is to make the coupling holes individually have less coupling variation with frequency; since the total coupling loss between two identical transmission lines is a function only of number of coupling holes and the loss per hole (equations (39) and (40)) constant coupling per hole will produce constant coupling overall. Riblet and Saad[6] have reported on this approach.

There is another approach to obtaining flat coupling versus frequency despite variations in the coupling per hole, and that is to intentionally create a difference between the phase constants of the two coupled lines. Fig. 17 illustrates the transfer characteristic when the coupled lines have unequal phase constant, and either identical or negligible attenuation constants. Near the maximum for the transferred wave $| E_2^* |$ there is a region wherein the transfer loss is independent of coupling strength, and the transfer loss in this flat-loss region is under control of the ratio $(\beta_1 - \beta_2)/c$. Hence for a given transfer loss there is an optimum ratio of phase constant difference to coupling strength in order to minimize the overall transfer loss variation. For the distributed coupling case, equations (31) and (32) represent the transferred wave amplitude and show that the transferred wave goes through a maximum as a function of integrated coupling strength $\underline{cx}$, when

$$\sqrt{\frac{(\beta_1 - \beta_2)^2}{4c^2} + 1}\, cx = \frac{\pi}{2} + n\pi. \tag{42}$$

The transferred amplitude at this maximum point is

$$E_{2\,\max}^* = \frac{1}{\sqrt{\dfrac{(\beta_1 - \beta_2)^2}{4c^2} + 1}}. \tag{43}$$

The integrated coupling strength at the maximum point is

$$c_0 x_0 = \frac{1}{\sqrt{\dfrac{(\beta_1 - \beta_2)^2}{4c^2} + 1}} \cdot \frac{\pi}{2}. \tag{44}$$

For the important case of an optimum 3 db transfer loss coupler, E_2^* is 0.707. Then $(\beta_1 - \beta_2)/c$ equals 2 and $\underline{c_0 x_0}$ equals $\pi/2\sqrt{2}$ from (43)

and (44). Assuming a coupling length x_0 of two wavelengths in the line with the smaller phase constant, it follows that β_1/β_2 is about 1.18 showing that a phase-constant difference of 18 % is required. This phase-constant difference is quite readily attainable in the waveguide structure of Fig. 50(a). The two modes coupled together are given slightly different cut-off wavelengths in the coupling region, and may be tapered to the standard waveguide size outside the coupling region. The desired phase-constant difference can also be obtained in two identical metallic guides by inserting a piece of dielectric into one of the guides in the coupling region as sketched in Fig. 50(b). Although rectangular waveguides are used in Fig. 50 to illustrate the method of obtaining frequency independent transfer characteristics, the approach is general and may be applied to any form of single or multi-mode transmission line.

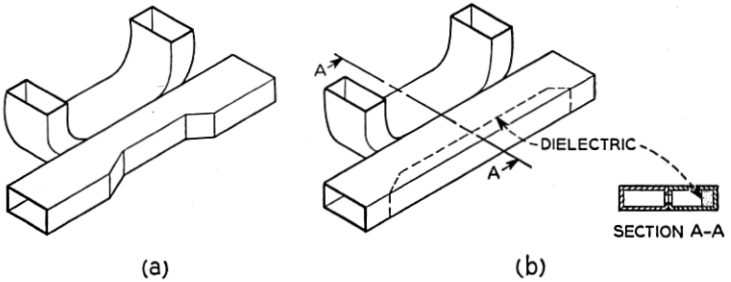

Fig. 50 — Examples of structures in which flat transfer loss may be obtained despite coupling loss variations.

In either dominant-mode directional couplers or in multi-mode coupled-wave devices such as the one illustrated in Fig. 1, one may obtain much more frequency selectivity than occurs incidentally due to the frequency sensitivity of the coupling elements used. This may be done by coupling two transmission lines which have the same phase constant at one frequency, but unequal phase constants at other frequencies. Then, as shown by equation (31), the midband transfer loss may be set at any desired value by adjusting the integrated coupling strength $\underline{cx}$ at midband (where $\beta_1 - \beta_2 = 0$), and at other frequencies where $(\beta_1 - \beta_2) \neq 0$, the transfer loss will increase. For the particular case of $\underline{cx} = \pi/2$ (fixed) for which complete power transfer occurs when $\beta_1 = \beta_2$ (and assuming $\alpha_1 = \alpha_2$ or both α's are negligible), Fig. 51 shows the shape of the filter characteristic, E_2^* versus $(\beta_1 - \beta_2)/2c$. This plot is valid for any form of transmission line.

A very simple configuration for realizing such a frequency-selective filter involves coupling between two hollow conductor waveguides, one

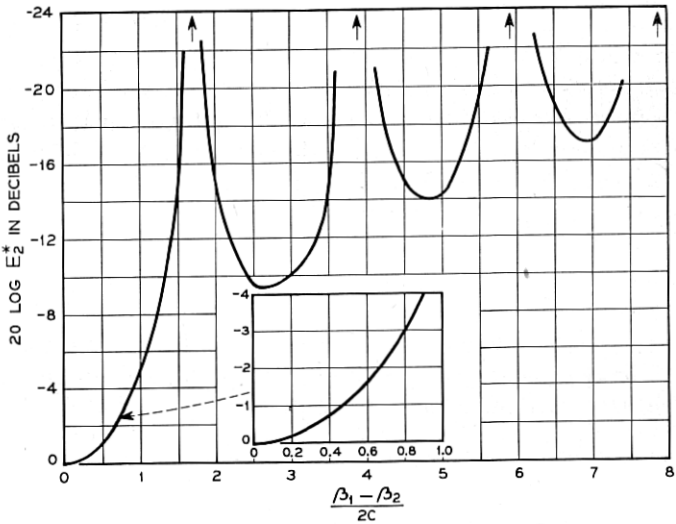

Fig. 51 — Transfer loss E_2^* versus $(\beta_1 - \beta_2)/2c$ for coupling strength $cx = \pi/2$, the value required for complete power transfer.

of which is air-filled and the other of which is filled with a material of dielectric-constant ϵ. The phase constants for these waveguides have the form sketched in Fig. 52, in which β_0 is the phase constant in free space. At the frequency f_m the two waveguides have identical phase constants and, in a typical case, negligible loss constants so that complete power transfer can be obtained. For the case $\epsilon = 2.55$, Fig. 53 shows the computed frequency characteristic on the assumption that the integrated coupling is set for complete transfer ($cx = \pi/2$) and is independent of frequency. (Actually the usual coupling mechanisms are somewhat frequency sensitive and would increase the selectivity somewhat.) This filter

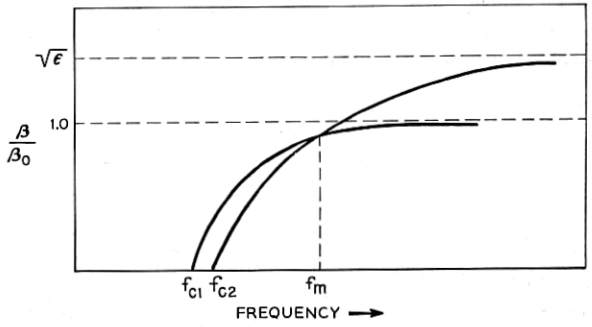

Fig. 52 — The general form of the phase constants for two hollow conductor waveguides, one of which is filled with a dielectric.

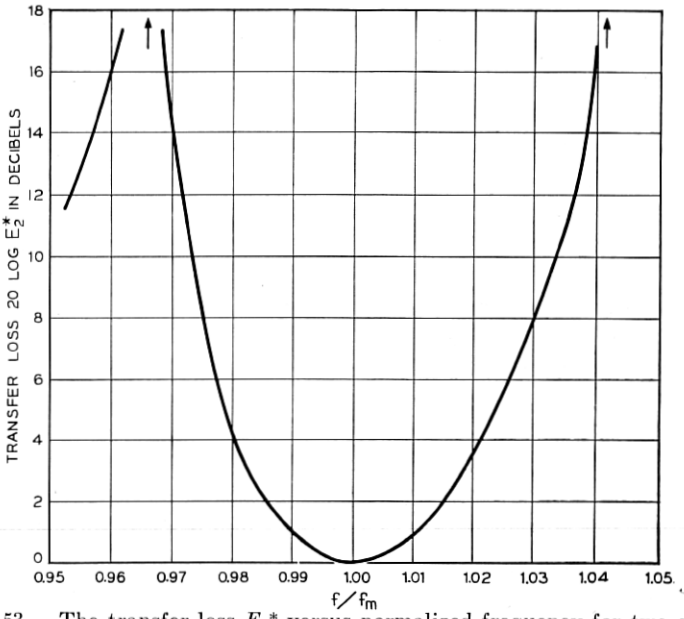

Fig. 53 — The transfer loss E_2^* versus normalized frequency for two coupled hollow conductor waveguides, one of which is air filled and has a guide wavelength $\sqrt{2}$ times the free space wavelength at f_m , and the other of which is filled with a material of dielectric constant 2.55 with dimensions chosen for equality of phase constant with the air-filled guide at f_m . Coupling $\underline{cx}$ assumed constant at $\pi/2$.

characteristic applies regardless of the shapes of the hollow conductor waveguidess (which may be dissimilar) and regardless of the modes selected.

It is apparent that frequency selectivity in the transfer characteristic E_2^* can also be obtained without requiring that the phase constants be unequal by using coupling elements which are frequency sensitive.

DIELECTRIC WAVEGUIDE CONFIGURATIONS

The coupled-wave approach to circuit design is applicable using any form of transmission line, the only important variant associated with different forms of line being the physical structure associated with introducing the desired coupling between lines. In a recent publication[8] A. G. Fox showed that dielectric waveguides are very attractive for use in the millimeter wavelength range, and this section points out how dielectric waveguides can be used in various forms of coupled wave devices. Fox showed that dielectric waveguides arranged in the configuration sketched in Fig. 54 are coupled by the electric field components only, and that

periodic energy exchange of the type described by equations (26) and (27) is observed. Moreover, he also showed that if one line were made very lossy the energy exchange phenomena disappeared and, despite sufficient coupling to cause complete power transfer when both lines were loss-free, power passed through the coupling region in the low-loss line with less than 0.25 db attenuation. This verified the predictions of equations (35) and (36).

Other implications of the coupled wave theory can also be utilized in dielectric waveguides. If the two lines (Fig. 54) are made of materials having different dielectric constants and their cross-sectional dimensions set so as to secure identical phase constants at a frequency f_m, then a frequency-selective coupled-wave filter results and the selectivity characteristic of Fig. 53 applies. As an alternative to using materials having different dielectric constants, the same dielectric may be used for both lines by making one line solid and the other hollow.

If both lines are made of the same material and the cross-sectional dimensions are set so as to obtain a known difference between their phase constants, the result is a directional coupler having a region of flat transfer loss (of any desired magnitude) and equations (42), (43) and (44) apply.

Both of the preceding applications can be carried out in dielectric waveguides having arbitrary cross-sectional shapes.

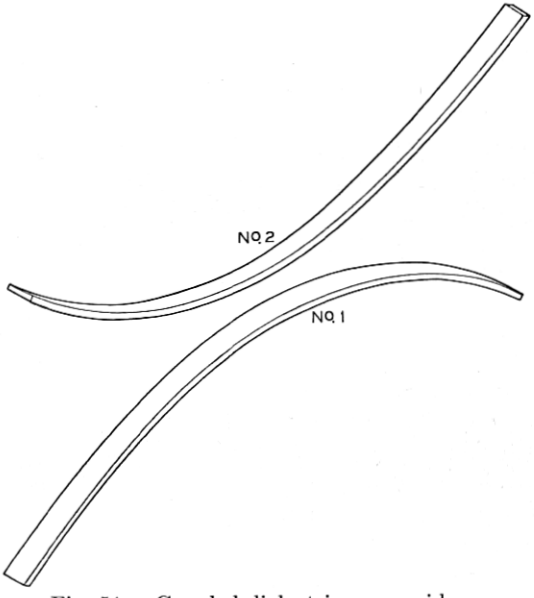

Fig. 54 — Coupled dielectric waveguides.

If one of the transmission lines (Fig. 54) is round and the other is rectangular and if their cross-sectional dimensions are set for equal phase constants, then the power in one of the two polarizations of the round line may be transferred to any desired extent to the rectangular guide, and power in the other polarization of the round guide will pass the coupling region undisturbed. Two such rectangular-rod to round-rod coupling configurations arranged in cascade along the round-rod, with the two rectangular rods coupled in planes at 90° to each other, constitutes a means for independently connecting to the two polarizations of the round-rod. This type of device depends upon the fact that the phase constants of the two polarizations of round-rod are identical, whereas the two phase constants for the rectangular rod are different. Thus a wave interference occurs in the transfer characteristic for one of the polarizations, and for suitable values of $(\beta_1 - \beta_2)/c$ (see Fig. 18) the power transferred in this polarization can be made small.

SUMMARY

Two approaches to a theoretical description of the behavior of two coupled waves have been presented. One, based on the assumption of negligibly small coupling, is applicable in cases where very little power is transferred between the coupled waves. The other, a solution based on uniform coupling between waves in the coordinate of propagation, is valid for any magnitude of total coupling.

The loose coupling theory shows how to taper the coupling distribution in order to minimize the length of the coupling interval required for a given degree of directivity and/or for a given magnitude of mode impurity. In particular, it is possible to shape the coupling distribution so as to discriminate sharply against one or more undesired modes in a coupled-wave arrangement involving just a few modes. (See Figs. 7 and 15 for examples).

The theory indicates that significant exchange of power takes place provided that the attenuation and phase constants of the coupled waves are equal, or provided that the difference between the attenuation constants and the difference between the phase constants are small compared to the coefficient of coupling. A suitable difference between either the attenuation constants or the phase constants of two coupled waves is sufficient to prevent appreciable energy exchange (equations 29–32 and 35–36).

It follows that substantially single-mode propagation is possible in a multi-mode structure even though geometrical effects tending to cause coupling between modes are present. A gradual transition in the boundary

of a multi-mode waveguide will not cause an appreciable exchange of power between modes provided that the quantity $(\beta_1 - \beta_2)/c$ is sufficiently large for the modes which are coupled by the boundary change. Similarly, for disturbances in the coupled-wave system which takes place over a large number of wavelengths in the direction of propagation, the coupled-wave theory indicates that all conversion will take place in the forward direction and very little reflection in any mode will result.

The tight coupling theory shows that for the case of identical complex propagation constants, a periodic exchange of energy between waves takes place along the coordinate of propagation. The only effect of the existence of an attenuation constant for both waves (compared to the dissipationless case) is to add the same exponential attenuation factor (to the periodic energy exchange phenomenon) which would have existed for a wave traveling on one of the lines in the uncoupled state.

When the phase constants of the two coupled waves are not equal (and the attenuation constants are either equal or negligibly small compared to the coupling coefficient), the exchange of energy between waves is no longer complete but remains periodic (Fig. 17). The quantity $(\beta_1 - \beta_2)/c$ determines the fraction of the total energy which is exchanged, and also modifies the period of the energy exchange phenomenon along the axis of propagation.

When the phase constants of the two lines are equal but the attenuation constants are unequal, the energy transfer phenomenon differs only slightly from that associated with equal propagation constants provided that the quantity $(\alpha_1 - \alpha_2)/c$ is less than about -0.1. For $(\alpha_1 - \alpha_2)/c$ more negative than about -1, the periodicity of the energy transfer phenomenon has largely disappeared (Fig. 23) and as $(\alpha_1 - \alpha_2)/c$ becomes on the order of -10 or more, the principal effect of the coupling for the low loss line is a minor alteration of the phase and attenuation constants. The wave amplitude for unit input on the low-loss line becomes [from (33) for $|(\alpha_1 - \alpha_2)|/c \gg 1$]

$$E_1 = \epsilon^{-[\alpha_1 - c^2/(\alpha_1 - \alpha_2) + i(c+\beta)]x}. \tag{45}$$

Through proper choice of the phase constants relative to the coupling coefficient in two coupled transmission lines, it is possible to make directional couplers having an arbitrary transfer loss that is independent of frequency despite variations in coupling strength with frequency (equations 43–44). It was also shown that the coupled-wave approach may be utilized to create highly frequency-selective filters which may operate between single-mode media or between selected individual modes of a multi-mode system.

The experimental data given for two dominant-mode rectangular waveguides showed that the periodic energy exchange theoretically predicted for a coupled-wave system can be achieved in coupled transmission lines.

Performance characteristics were given for some loosely coupled transducers between a dominant-mode rectangular waveguide and one mode of a six-mode waveguide. A tapered coupling distribution was used to achieve the mode selectivity in a limited length interval.

The problems associated with a coupled-wave transducer for transferring all of the power from a dominant-mode rectangular waveguide to the circular electric mode in a ten mode waveguide, were discussed and the observed characteristics of an experimental model were given.

The application of coupled-wave techniques to other types of transmission systems was illustrated by pointing out analogous structures using coupled dielectric waveguides.

ACKNOWLEDGMENT

The writer is indebted to W. W. Mumford for helpful discussions during the early stages of this work; to R. W. Dawson who made most of the measurements on the models of Figs. 36 through 44, and to G. D. Mandeville who made measurements on the model of Fig. 39.

BIBLIOGRAPHY

1. S. E. Miller and A. C. Beck, Low-Loss Waveguide Transmission, Proc. I.R.E., **41,** pp. 348–358, Mar., 1953.
2. S. E. Miller, Notes on Methods of Transmitting the Circular Electric Wave Around Bends, Proc. I.R.E., **40,** pp. 1104–1113, Sept., 1952.
3. W. W. Mumford, Directional Couplers, Proc. I.R.E., **35,** pp. 160–165, Feb., 1947.
4. C. L. Dolph, A Current Distribution for Broadside Arrays Which Optimizes the Relation Between Beam Width and Side Lobe Level, Proc. I.R.E., **34,** pp. 335–348, June 1946.
5. S. E. Miller and W. W. Mumford, Multi-Element Directional Couplers, Proc. I.R.E., **40,** pp. 1071–1078, Sept., 1952.
6. H. J. Riblet and T. S. Saad, A New Type of Waveguide Directional Coupler, Proc. I.R.E., **36,** pp. 61–64, Jan., 1948.
7. M. Arnoff, Radial Probe Measurements of Mode Conversion in Large Round Waveguide with TE_{01} Excitation, (submitted to Proc. I.R.E.).
8. A. G. Fox, New Guided Wave Techniques for the Millimeter Wavelength Range, given orally at the March, 1952, I.R.E. National Convention. To be submitted to the Proceedings.
9. Alan A. Meyerhoff, Interaction Between Surface-Wave Transmission Lines, Proc. I.R.E., **40,** pp. 1061–1064, Sept., 1952.
10. P. E. Krasnushkin and R. V. Khokhlov, Spatial Beating in Coupled Waveguides Zh. Tekh. Fiz, **19,** pp. 931–942, Aug., 1949, (in Russian).
11. W. J. Albersheim, Propagation of TE_{01} Waves in Curved Wave Guides, B.S.T.J., **27,** pp. 1–32, Jan., 1949.